Diagnostics of Plasma-Produced Hydrogen Peroxide in Liquids

Diagnostik von plasmaerzeugtem
Wasserstoffperoxid in Flüssigkeiten

Bachelor Thesis

in the
Degree Program
„Bachelor of Science“
in Physics

at the Faculty of Physics and Astronomy
of the Ruhr-Universität Bochum

by
Emanuel Jeß

from
Hattingen

Bochum 2022

Abstract

In project B11 which is part of the Collaborative Research Center 1316 (CRC1316) funded by the German Research Foundation (DFG) the goal is to optimize plasma and liquid chemistry for biocatalysis. In biocatalysis enzymes are used as catalysts which leads to reduced waste and safer processes. For the investigated biocatalytic reaction, the enzymes require hydrogen peroxide but are inactivated by large amounts of it. A solution for this problem is the in situ production with a plasma source. Hereby, a micro-scaled atmospheric pressure plasma jet is advantageous. A capillary plasma jet, which is derived of the COST reference plasma jet, is utilised as plasma source. The working gas (helium or argon) is mixed with wet helium or argon respectively which is piped through an ice-cooled bubbler system.

In this work, the hydrogen peroxide concentration in the plasma treated liquid was detected. In doing so, two diagnostics were applied: a spectrophotometric approach with the chemical ammonium metavanadate and an electrochemical approach using a Prussian blue coated electrode. The power dissipated in the plasma, the water admixture, the working gas (helium or argon), the total gas flow and the modulated frequency were varied and analysed regarding their influence on the hydrogen peroxide concentration.

It was found that helium yields higher hydrogen peroxide concentrations and a more stable discharge than argon. The hydrogen peroxide concentration increases towards higher powers up to 6 W where the concentration stagnates. Regarding the water admixture, the hydrogen peroxide concentration increases when adding more water to the gas flow. Although the slope of this curve decreases, a local maximum could not be observed for water concentrations up to (6700 ± 300) ppm and a power of 6 W. Furthermore, the hydrogen peroxide concentration increases linearly with the total gas flow and the treatment time. A maximal hydrogen peroxide concentration of 2 mM was observed after treating the liquid for 5 min at a power of 6 W, a water concentration of (6700 ± 300) ppm and a total gas flow of 2 slm. The frequency modulation increases the energy efficiency (up to $0.73\,\mathrm{mg\,kWh^{-1}}$) but needs further investigation. Similar results were obtained for a wider capillary, which yields higher hydrogen peroxide concentrations.

In sum, the capillary plasma jet proved to be a suitable plasma source for project B11. Furthermore, hypothesis regarding the production and loss processes of hydrogen peroxide for this plasma source could be generated. To cover the whole reaction pathway, the concentration of other reactive species like hydroxyl (OH) needs to be determined. Also the concentrations in the gas phase and effluent require additional investigation.

Zusammenfassung

Im Projekt B11 wird im Rahmen des Sonderforschungsbereichs 1316 (SFB1316) das Ziel verfolgt, die chemischen Prozesse im Plasma und in einer Flüssigkeit für die Biokatalyse zu optimieren. In biokatalytischen Prozessen werden Enzyme als Katalysatoren genutzt, um Abfälle zu reduzieren und die Sicherheit der Prozesse zu erhöhen. Die verwendeten Enzyme benötigen eine bestimmte Menge an Wasserstoffperoxid, da sie bei hohen Konzentrationen inaktiviert werden. Dieses Problem kann durch in situ Produktion mit einer Plasmaquelle gelöst werden. Dabei ist die Verwendung eines Mikroplasmajets bei Atmosphärendruck vorteilhaft. Als Plasmaquelle wird ein Kapillarenjet verwendet, der eine Weiterentwicklung des COST Referenzplasmajets ist. Ein Teil des Trägergas (Helium oder Argon) wird durch ein eisgekühltes Bubblersystem geleitet.

In dieser Arbeit wurde die Wasserstoffperoxidkonzentration in der behandelten Flüssigkeit detektiert. Dafür wurden zwei Diagnostiken verwendet: ein spektrophotometrisches Vorgehen unter Verwendung der Chemikalie Ammonium Metavanadat sowie ein elektrochemisches Vorgehen, bei dem eine mit preußisch blau beschichtete Elektrode eingesetzt wird. Es wurden die ins Plasma eingekoppelte Leistung, die Wasserbeimischung, das Trägergas (Helium oder Argon), der Gesamtgasfluss sowie die modulierte Frequenz variiert und bezüglich ihres Einflusses auf die Wasserstoffperoxidkonzentration analysiert.

Die Untersuchungen ergaben, dass die Verwendung von Helium als Trägergas zu höheren Wasserstoffperoxidkonzentrationen führt. Zudem steigt die Wasserstoffperoxidkonzentration mit zunehmenden Leistungen bis zu 6 W und stagniert dann. Durch Erhöhung der Wasserbeimischung im Gasfluss wird ebenfalls ein Anstieg der Wasserstoffperoxidkonzentration verursacht. Obwohl die Steigung dieses Graphen abnimmt, konnte kein lokales Maximum für Wasserkonzentrationen bis zu (6700 ± 300) ppm und eine Leistung von 6 W festgestellt werden. Weiterhin steigt die Wasserstoffperoxidkonzentration bei Erhöhung des Gesamtgasflusses. Insgesamt betrug die maximal beobachtete Wasserstoffperoxidkonzentration 2 mM nach einer Behandlungszeit von 5 min, einer Leistung von 6 W, einer Wasserkonzentration von (6700 ± 300) ppm und einem Gesamtgasfluss von 2 slm. Die Modulation der Frequenz steigert die Energieeffizienz (bis zu 0,73 mg kWh^{-1}), bedarf aber weiterer Untersuchungen. Ähnliche Ergebnisse wurden für eine breitere Kapillare erzielt, mit der höhere Wasserstoffperoxidkonzentrationen erzielt wurden.

Zusammengefasst erwies sich der Kapillarenjet als für das Projekt B11 geeignete Plasmaquelle. Zudem konnten aus den Ergebnissen Hypothesen über Produktions- und Verlustprozesse von Wasserstoffperoxid für den Kapillarenjet abgeleitet werden. Für das Verständnis der gesamten Reaktionskette muss die Konzentration anderer reaktiver Spezies, wie Hydroxyl (OH), bestimmt werden. Ebenfalls bedürfen die Konzentrationen im Plasma und Effluenten weitere Untersuchungen.

Contents

1 Introduction

This thesis contributes to project B11 which is part of the Collaborative Research Center 1316 (CRC1316) funded by the German Research Foundation (DFG). The goal of project B11 is to optimize plasma and liquid chemistry for biocatalysis [7]. In biocatalysis enzymes are used as catalysts because they exhibit high selectivity and accept various complex molecules as substrates [30]. Moreover, the use of enzymes results in reduced waste and inherently safer processes due to milder reaction conditions [33]. Therefore, biocatalysis meets the criteria of green and sustainable chemistry [33].

The department of Applied Microbiology uses the enzyme 'evolved recombinant unspecific peroxygenase from Agrocybe aergerita (rAaeUPO)' [44]. In the presence of hydrogen peroxide UPO hydroxylates the substrate ethylbenzene to the product (R)-1-phenylethanol. The enzymes require hydrogen peroxide but are inactivated by large amounts of it [44]. Thus, an in situ production of hydrogen peroxide is needed to adjust the concentration gradually and simultaneously prevent the dilution of the reaction solution [44]. There are several approaches to realize the in situ production of hydrogen peroxide [44]: enzyme cascades [20], light-activated flavins [9], photo catalysts [34] and electrochemistry [23]. In project B11 a micro-scaled atmospheric pressure plasma jet (μ-APPJ) is applied to treat the reaction solution [45], because it does not induce additional costs by adding more components, especially enzymes, to the reaction. Moreover this method is non-invasive, unlike the electrochemical approach [44]. In the latter electrodes are immersed in the solution which can cause precipitation of buffer salts and enzymes [44]. Yayci et al. summarized that a 'noninvasive in situ approach [...] would present a significant advantage' [44].

In the course of the project, the reaction pathways of hydrogen peroxide and other reactive species, such as hydroxide, are to be understood by analysing the gas phase, the effluent and the liquid phase [7]. The concentrations of other reactive oxygen species (ROS), apart from hydrogen peroxide, are of interest because other ROS can deactivate the enzymes as well or potentially consume the substrate [7].

During this thesis, the hydrogen peroxide concentration in the liquid was investigated. Considering the sensibility of the enzymes to the hydrogen peroxide concentration in the liquid, its diagnosis is important for the biocatalysis setup. Furthermore, knowing the hydrogen peroxide concentration in the liquid leads to feasible working parameters, e. g. power dissipated in the plasma and water admixture in the gas flow, for the capillary jet. Moreover, by varying these working parameters, relations between the hydrogen peroxide concentration and those parameters can be discovered. Then it can be hypothesised how the working parameters influence production and loss processes of hydrogen peroxide in the plasma.

2 Theory

This chapter gives an overview over special characteristics of the plasma source. Additionally, plasma chemistry regarding the hydrogen peroxide production is thematised. Finally, research questions are deduced.

2.1 Atmospheric pressure plasmas and RF discharges

Before the special characteristics of atmospheric pressure plasmas will be discussed, a brief introduction and categorization of plasmas in general is given. Chen uses a popular definition of a plasma:

> 'A plasma is a quasineutral gas of charged and neutral particles which exhibits collective behavior [sic].' (Chen, p. 2) [6]

In this definition the terms 'quasineutral' and 'collective behaviour' need further explication. Quasineutrality stands for the shielding of the plasma bulk against external potentials or local charge concentrations [6]. To see this plasma behaviour, the length scale (Debye length λ_D) should be much smaller than the dimension of the system (L) [6]. Collective behaviour means that the motion of particles is not only influenced by local but also by remote regions of the plasma [6]. This requires the number of particles in the Debye sphere N_D to be much higher than 1 [6]. The third condition for a plasma is that electromagnetic forces are more important than collisions with neutral atoms [6]. Plasmas are often categorized by the number density of charged particles, such as electrons and ions, and their energy distribution (often referred to as temperature), e. g. in [29].

Unlike low-pressure plasma sources, atmospheric pressure plasma sources do not require vacuum chambers and pumps [39]. This is advantageous for applications like polymeric surface modification, bacterial and biomolecule inactivation or wound healing [39]. In this work, the enzymes used for biocatalysis require mild working conditions [33]. Therefore, low pressure plasma sources are not an option for the desired in situ approach.

In the following atmospheric pressure plasmas are described and the characteristics of helium and argon discharges are summarized. The voltage needed to ignite the plasma between two electrodes depends on the pressure p and the gap d and is described by Paschen's law [6]. In case of an atmospheric pressure plasma, the pressure is constant. Thus, the dimension of the plasma needs to be adjusted. Typical gap sizes amount to several millimetres [36]. The plasmas source used in this thesis is a micro-scaled atmospheric pressure plasma jet (μ-APPJ) with a glass capillary inserted between the electrodes. Typically, a μ-APPJ consists of two electrodes with a working gas flowing between them [40]. Usually helium is utilised as working gas because homogeneous discharges can be generated easily with helium [10]. However, argon seems to be more beneficial for certain chemical processes [10], e. g. higher energy efficiency in hydrogen peroxide production [38]. The Paschen curves for a RF discharge show that argon as working gas needs higher voltages than helium [27]. Moreover, differences between argon and helium occur not only at ignition. For the COST-jet, Golda et al. report higher electron densities but lower electron temperatures in the argon discharge compared to the helium discharge [10]. Helium is lighter than argon which causes lower electron densities in helium discharges [19]. This is due to either higher losses because of diffusion for small plasma dimensions or better heat transfer from electrons to heavy particles for large dimensions [19].

The utilised plasma source is operated with alternating voltage. Hereby, the risk of arcing, compared to DC voltage, is decreased due to lesser currents between the electrodes. This is further reduced by inserting the capillary. A DC discharge with a dielectric and constant voltage would extinguish once charges accumulate on the dielectric. Moreover, the applied frequency amounts to 13.56 MHz and is part of the radio frequency (RF) spectrum. Different operating regimes are described for RF discharges [43]. They are denoted as α-like and γ-like mode due to the emission structure which is comparable to their low pressure pendants [12]. Hemke et al. investigated the physical properties of the α-like mode of RF discharges and found out that the ionization is mainly caused by ohmic heating in the bulk [16]. The γ-like mode in RF discharges is caused by Penning ionisation within the sheaths [3]. For this reason, Bischoff et al. proposed the name Penning mode [3]. Penning ionisation denotes a collisional process between excited (A^*) and ground state species (B) which results in ionisation of the latter and relaxation of the excited species [18]:

$$\mathrm{A^* + B \longrightarrow A + B^+ + e^-} \tag{2.1}$$

On the one hand, the electrons resulting from Penning ionisation are accelerated in the sheath electric field towards the plasma bulk [3]. However, the multiplication of these electrons by electron cascades is limited because the Penning ionisation occurs at the edge of the sheath close to the bulk [3]. On the other hand, the ions created by Penning ionisation can cause emission of secondary electrons at the electrode [3]. These electrons are also accelerated through the sheath towards the bulk and multiplicate collisionally in the sheath [3]. Additionally, the discharge can become constricted which is referred to as the 'arcing mode' [32]. Because of the dielectric (glass), the capillary jet should not operate in arcing mode.

Added to the aforementioned plasma parameters and operation modes, plasmas are categorized according to the existence of thermodynamic equilibrium [36]. Local thermodynamic equilibrium (LTE) and non-local thermodynamic equilibrium (non-LTE) states are distinguished [36]. In the first the temperature of electrons and heavy particles is about the same (e. g. 10^4 K) [36]. In non-LTE plasmas the electron temperature (e. g. 10^4 K to 10^5 K) is significantly higher than the temperature of heavy particles (e. g. 300 K to 1000 K), such as ions [36]. The capillary jet produces a non-LTE plasma with high electron temperatures and gas temperature [41]. The lack of a thermodynamic equilibrium and an admixture of molecular gases or the contact with liquids yield a high amount of reactive species [4]. For example, plasmas in contact with liquids can produce hydroxyl (OH), atomic oxygen (O) and hydrogen peroxide (H_2O_2) [4]. The key processes of hydrogen peroxide production and destruction regarding the utilised setup are thematised in the following section 2.2.

2.2 Plasma chemistry

As mentioned before, key production and loss processes of hydrogen peroxide will be discussed later on in this section. In general, there can occur different reactions in the plasma between its species. Lieberman and Lichtenberg list a set of elementary reactions [24]:

- $e + AB \longrightarrow AB^+ + 2\,e$ (electron-ion pair production),
- $e + AB \longrightarrow e + A + B$ (radical production/dissociation),
- $e + AB \longrightarrow A^- + B$ (negative ion production),
- $A + B \longrightarrow C + D$ (gas-phase chemical reactions),
- and transport to surfaces as well as surface-phase reactions.

The net energy necessary for all reactions has to be coupled into the plasma by the power source [24]. A chemical system can be either in a thermodynamic equilibrium or a non-thermodynamic equilibrium state [24]. In the case of the atmospheric pressure discharge, the system is not in a thermal equilibrium because the electron and atom temperature differ (see section 2.1). Then the reactions can be described by rate constants, the density of the species and its temporal derivation [24]. For example, the following reaction between A and B is considered [24]:

$$\mathrm{A} \xrightarrow{k_\mathrm{A}} \mathrm{B} \tag{2.2}$$

Then the densities $n_{\mathrm{A,B}}$ can be described by the differential equations:

$$\frac{\mathrm{d}n_\mathrm{A}}{\mathrm{d}t} = -k_\mathrm{A} n_\mathrm{A} \tag{2.3}$$

$$\frac{\mathrm{d}n_\mathrm{B}}{\mathrm{d}t} = k_\mathrm{A} n_\mathrm{A} \tag{2.4}$$

The rate constants often depend on the energy distribution or temperature of the reactants [24].

After some aspects of plasma chemistry were summarized above, the processes regarding hydrogen peroxide are considered. In a simulation study the chemical processes of a μ-APPJ with a gas flow of wet helium are investigated by Liu et al. [25]. Two regimes were considered: one for low water concentrations (1 ppm to 30 ppm) and one for higher water concentrations (30 ppm to 3000 ppm) [25]. At low water concentrations (first regime) the discharge consists mainly of helium species [25]. In the second regime water related species dominate over helium species and the electronegativity increases [25]. In another work Vasko et al. investigated specifically the processes regarding hydrogen peroxide in the context of the simulation study [38]. They compared the simulation to experimental results for a discharge across a 1 mm gap, at 2.78 W ($1.59\,\mathrm{W\,cm^{-2}}$) with 13.5 MHz, a water admixture of 0.47 %, a total gas flow of 2 slm and a gas temperature of 348 K [38]. The comparison indicated that the following three body association process is mainly (99.60 %) responsible for the production of hydrogen peroxide:

$$\mathrm{OH} + \mathrm{OH} + \mathrm{M} \xrightarrow{k_1} \mathrm{H_2O_2} + \mathrm{M} \tag{2.5}$$

with a heavy particle M (e. g. helium). The rate constant for the reaction above (equation (2.5)) $k_1 = 3.7 \times 10^{-43}(T_\mathrm{gas}/300)^{-0.8}$ decreases with gas temperature T_gas [8, 37]. The main (42.92 %) loss process of hydrogen peroxide also depends on hydroxyl (OH) [38]:

$$\mathrm{OH} + \mathrm{H_2O_2} \xrightarrow{k_2} \mathrm{H_2O} + \mathrm{HO_2} \tag{2.6}$$

with the rate constant $k_2 = 2.88 \times 10^{-12} \exp(-156.3/T_\mathrm{gas})$ [17]. The rate constant for equation (2.6) increases with gas temperature [17]. In contrast to the production process, more than one principal process contributes to the destruction of hydrogen peroxide [38]. For example, other processes are radial losses (25.98 %), electrode losses (11.78 %) or several collisions with electrons (11.44 % + 2.90 % + 0.57 %) and collisions with hydrogen (3.55 %) [38]. For the hydroxyl, the main production process is the dissociation of water molecules by electrons (43.99 %) [38]:

$$\mathrm{e} + \mathrm{H_2O} \xrightarrow{k_3} \mathrm{H} + \mathrm{OH} + \mathrm{e} \tag{2.7}$$

with the rate constant $k_3 = f(T_\mathrm{e})$ [26]. Unlike the rate coefficients k_1 and k_2, k_3 depends on a function of the electron temperature [26]. For the present plasma source the electron temperature presumably amounts to few electronvolts as for the comparable plasma source COST-jet an electron temperature of 1.7 eV was observed [10]. In this regime the rate constant k_3 increases with electron temperature and varies between $2.3 \times 10^{-18}\,\mathrm{m^3\,s^{-1}}$ and $1.8 \times 10^{-16}\,\mathrm{m^3\,s^{-1}}$ for electron temperatures between 1 eV and 2 eV [5]. The principal loss process for hydroxyl is the three body association reaction to hydrogen peroxide given by equation (2.5) [38]. If only the main production processes are considered and loss processes are neglected, two water molecules are needed to form one hydrogen peroxide molecule (see equation (2.7) and equation (2.5)).

In this work, only the detection of hydrogen peroxide in the liquid is conducted. Hence, the origin of the hydrogen peroxide is not determinable. But investigations regarding the origin (plasma, effluent or liquid) of reactive species show that hydrogen peroxide is primarily produced in the plasma [13, 14]. After being generated in the plasma, the species travel with the effluent to the liquid. Whether they transfer in equilibrium conditions from the gas to the liquid, depends on the Henry's law coefficient H [4]. For hydrogen peroxide, H is about $10^5\,\mathrm{M\,atm^{-1}}$ which indicates the hydrophilic character of hydrogen peroxide [4]. Thus, it is assumed that hydrogen peroxide molecules reaching the interface enter the liquid. Moreover, hydrogen peroxide is a long-lived species, which remains in the liquid after treatment [15].

2.3 Research questions

In section 2.1 and 2.2 important mechanisms and processes that could influence the hydrogen peroxide concentration were summarized. Starting from there, concrete research questions are deduced in the following. First of all, the variation of the power can influence not only the plasma parameters but also the gas temperature and operation mode (see section 2.1). Hence, with research question 1 (RQ1) this relation will be investigated:

RQ1

What is the relation between the power dissipated in the plasma and the hydrogen peroxide concentration?

For a similar setup, Vasko et al. reported an increase in the hydrogen peroxide concentration for higher powers [38]. Furthermore, the water admixture should have an effect on the hydrogen peroxide concentration as well because two water molecules are needed to produce one hydrogen peroxide molecule (see section 2.2):

RQ2

To what extend does the hydrogen peroxide concentration increase with the water admixture?

Because of the findings from Vasko et al., the hydrogen peroxide concentration should increase linearly up to water concentrations of 1 % (10 000 ppm) [38].

After varying power and water admixture with helium as working gas, similar measurements are conducted with argon. This could influence the hydrogen peroxide production as the working gas, inter alia, determines the plasma parameters electron temperature and density as well as the gas temperature. A comparison for different setups indicates that the use of argon as working gas could yield a higher energy efficiency [38]. This leads to research question 3 (RQ3):

RQ3

How does the working gas (helium or argon) influence the hydrogen peroxide concentration?

It is expected that argon could cause higher hydrogen peroxide concentrations because of the higher electron density. Furthermore, Vasko et al. found that variation of the total gas flow boosts the hydrogen peroxide production [38]. They attributed the effect to the decrease of the residence time with the total gas flow [38]. This is thematised by research question 4 (RQ4):

RQ4

In what way are shorter residence times beneficial to the hydrogen peroxide concentration?

Finally, the results of a 0D plasma-chemical kinetics simulation suggest that modulating the RF frequency could be beneficial to the hydrogen peroxide production [7]. This raises the following question:

RQ5

How does the frequency modulation change the production of hydrogen peroxide?

It is assumed that longer lived species, such as hydrogen peroxide, are accumulated in the discharge volume while short lived species like hydroxyl (OH) diminish as soon as the plasma is turned off [7].

In sum, the following parameters will be investigated regarding their influence on the hydrogen peroxide concentration in the liquid: power, water admixture, working gas, total gas flow/residence time and frequency modulation.

3 Experimental Methods

In this chapter the plasma source and two diagnostics to detect hydrogen peroxide in the liquid are introduced. As diagnostics a spectrophotometric and an electrochemical approach are employed. Furthermore, the utilised method to determine the evaporation of the liquid is presented.

3.1 Plasma source

The plasma source is a micro-scaled atmospheric pressure plasma jet (μ-APPJ). During the first funding period of the CRC1316, a proof of principle for the plasma driven biocatalysis was performed [44]. In subsequent investigations the μ-APPJ was found to be more beneficial than a dielectric barrier discharge (DBD) because larger volumes can be treated directly with its effluent [45]. As μ-APPJ, the COST (Cooperation in Science and Technology) Reference Plasma Jet (COST-jet) was used. The COST-jet is designed to serve as a reference plasma source to make comparisons between different plasma sources possible [11]. In project B11 the COST-jet is replaced by a capillary plasma jet due to the latter's higher variability regarding the effective plasma volume and operational parameters [41]. Winzer et al. characterized a structurally identical capillary plasma jet and found it to function similar to the COST-jet [41]. Between the electrodes of the capillary plasma jet a glass capillary is inserted (see figure 3.1). Capillaries of two different sizes were compared concerning the production of hydrogen peroxide. The small capillary (CM Scientific) possesses a cross section of $1.4\,\mathrm{mm} \times 1.4\,\mathrm{mm}$ with a wall thickness of $0.2\,\mathrm{mm}$. This yields a plasma volume of $40\,\mathrm{mm}^3$. The cross section of the wide capillary (Hilgenberg) measures $(5.0 \pm 0.2)\,\mathrm{mm} \times (1.3 \pm 0.2)\,\mathrm{mm}$ with a wall thickness of $0.2\,\mathrm{mm}$. The plasma width for the wide capillary is smaller than the width of the capillary itself due to the slightly smaller electrodes ($(3.9 \pm 0.1)\,\mathrm{mm}$). The plasma volume amounts to $165.6\,\mathrm{mm}^3$. Both capillaries are longer than the electrodes ($40\,\mathrm{mm}$), so that the plasma does not cover the whole length of the capillary.

In the following, the setup for the operation of the capillary plasma jet, which is illustrated in figure 3.2, is described. The power is coupled into the plasma with an RF generator ($13.56\,\mathrm{MHz}$, Coaxial Power Systems) and a matchbox (Coaxial Power Systems MMN 150-13). To monitor the power dissipated in the plasma, voltage and current are measured with a high-speed oscilloscope (Teledyne LeCroy HDO6104A,

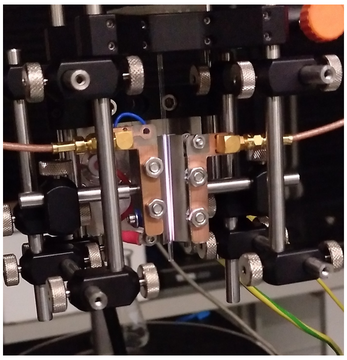

(a) Photograph.

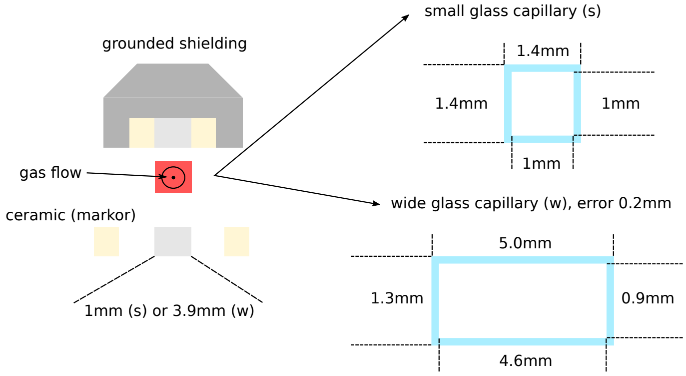

(b) Sketch.

Figure 3.1: Photograph of the jet and sketch of the electrodes and their housing.

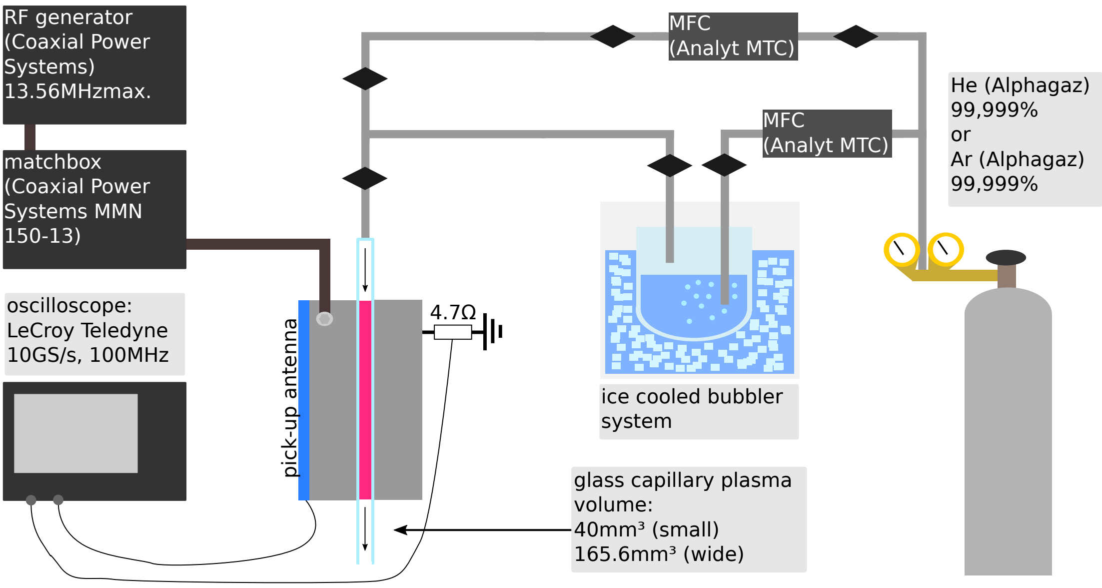

Figure 3.2: Sketch of the setup for the capillary plasma jet.

10GS/s, 1 GHz). For the voltage measurement a pick-up antenna is placed behind the powered electrode and the induced voltage is measured. By connecting a high voltage probe (Tektronix P5100A) to the powered electrode, a calibration factor for the voltage can be obtained (e. g. 170 for the small capillary). After readjusting the electrodes or changing the capillary, the calibration factor was redetermined. For the current measurement, a 4.7 Ω resistor is connected to the other electrode and the ground. The oscilloscope measures the voltage dropped across the resistor and the current can be calculated via Ohm's law (see also [11]). The power is calculated by determining the phase shift between current and voltage ($\Delta\phi$) via a function fit [11]. Then its substituted in the following equation:

$$P = U_{\text{rms}} \times I_{\text{rms}} \times \cos\left(-\frac{\pi}{2} + \Delta\phi - \Delta\phi_0\right) \tag{3.1}$$

with the effective values for voltage U_{rms} and current I_{rms} as well as the reference phase shift $\Delta\phi_0$ [12]. The ignition voltage usually lies between 200 V and 300 V depending on the water admixture. At a power of 10 W the measured voltage (rms) ranges from 550 V to 650 V. For some measurements the generator was operated in pulse mode to modulate the RF frequency. In doing so, a function generator (Tektronix AFG 3011) was connected to the generator and the duty cycle and the frequency of the pulse were varied. The generator needs a starting time of about 10 µs to ramp-up the voltage. In all measurements terminal resistors (Huber + Suhner AG, 50 Ω) were used to avoid a distortion of the signals.

In this paragraph, the gas supply and equations to calculate the water concentration in the gas flow are described. The gas supply consists of two mass flow controllers (Analyt MTC, 2 slm maximal gas flow), an ice cooled bubbler system and several valves (see figure 3.2). Helium (Alphagaz, 99.999 %) and argon (Alphagaz, 99.999 %) are used as working gases. The ice and water mixture is composed of 0.9 L ice cubes and 0.45 L fridge cooled water. The vessel is isolated and the temperature inside the bubbler (distilled water) was constant at 1.5 °C for several hours (not shown). To determine the concentration of water vapour in the gas flow, the vapour pressure over water is needed. It can be approximated by the following equation [1]:

$$p_{\text{vapour}}(T \text{ [in °C]}) \text{ [in hPa]} = 6.1094 \times e^{17.625T/(243.04+T)} \tag{3.2}$$

with the temperature of the water T and the vapour pressure over water p. For convenience equation (3.2) is multiplied with 100 to obtain the pressure in Pa. Then the result is computed with the following equation, which yields the concentration of water vapour in the gas flow [2]:

$$c_{\text{H}_2\text{O, gas}} = \frac{\phi_{\text{bubbler}}}{\phi_{\text{total}}} \times \frac{p_{\text{vapour}}(T)}{p_{\text{total}}} \times 10^6 \tag{3.3}$$

with the gas flow ϕ and the total pressure p_{total}. The total pressure is given by the atmospheric pressure $p_{\text{water}} = 101\,325$ Pa. The reason for this is that during operation the gas flows through the pipes and the jet to the atmosphere. The factor 10^6 is added for convenience to report the results in ppm. The propagation of uncertainty was calculated for the concentration:

$$\Delta c_{H_2O,\, gas} = \Delta T \frac{\phi_{bubbler}}{\phi_{total}} \times \frac{p_{vapour}(T)}{p_{total}} \times \frac{p_{vapour}(T)}{p_{total}} \times 10^6 \times \frac{17.625 \times 243.04}{(T + 243.04)^2} \quad (3.4)$$

with the uncertainty of the concentration $\Delta c_{H_2O,\, gas}$ and the uncertainty of the temperature $\Delta T = 0.5\,°C$. The uncertainty of the mass flow controllers and the atmospheric pressure were neglected because the temperature in the bubbler should yield the highest uncertainty.

3.2 Spectrophotometric approach with ammonium metavanadate

The spectrophotometric approach utilizes the colour change of the ammonium metavanadate (NH_4VO_3) solution in presence of hydrogen peroxide [28]. Its quantification is measured by absorption spectroscopy. Advantages of this method are the direct response to hydrogen peroxide, the stability of the solution and its ease of use [28].

3.2.1 Concept

The spectrophotometric approach relies on the reaction between hydrogen peroxide (H_2O_2) and metavanadate (${VO_3}^-$) [28]:

$$ {VO_3}^- + 4\,H^+ + H_2O_2 \longrightarrow {VO_2}^{3+} + 3\,H_2O \quad (3.5)$$

As product of the reaction above a red-orange colour peroxovanadium cation (${VO_2}^{3+}$) is formed, causing the liquid to change its colour and absorptivity [28]. The indicated colour variation is depicted in figure 3.3. The cuvette in the middle contained the highest concentration of hydrogen peroxide and the cuvette to the right contains the ammonium metavanadate solution without hydrogen peroxide. Because the reaction occurs in acidic medium, sulphuric acid (H_2SO_4) is mixed with ammonium metavanadate [28]. Nogueira et al. investigated this method and found the lowest amount of reagents with the highest absorbance signal to be [28]:

- H_2SO_4: $0.058\,mmol\,L^{-1} = 0.058\,mM$
- NH_4VO_3: $6.2\,mmol\,L^{-1} = 6.2\,mM$

To prepare a solution with the concentrations above, the mass of ammonium metavanadate (H_4NO_3V, therma scientific, 99.5 %) and the volume of sulphuric acid (H_2SO_4, Fisher Chemical, > 95 %) were calculated for a specific solution volume. For a solution volume of 1 L distilled water, the multiplication of the molar concentration with the molar mass $116.978\,g\,mol^{-1}$ (H_4NO_3V) and $98.08\,g\,mol^{-1}$ (H_2SO_4) results in a mass of 725.2636 mg (H_4NO_3V) and a volume of 3.109 mL (H_2SO_4, using

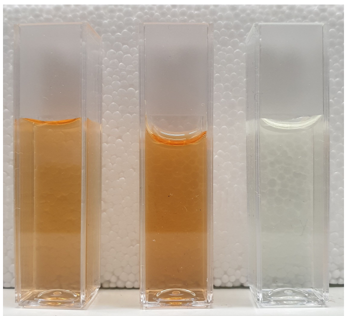

Figure 3.3: Example for the colour change of the liquid (left and middle: different H_2O_2 concentrations, right: ammonium metavanadate solution without H_2O_2).

the density $1.83\,\mathrm{g\,cm^{-3}}$). Adding the ammonium metavanadate to the magnetically stirred sulphuric acid solution led to less ammonium metavanadate stuck to the bottom of the beaker. The beaker is heated to 50 °C until the solution changes its colour to a red-orange shade [28]. The solution is then added to the desired volume of distilled water [28]. In doing so, the colour of the solution changes to a light yellow [28].

Additionally, Nogueira et al. report that the detection of hydrogen peroxide works properly between 0.143 mM and 5 mM [28]. At a hydrogen peroxide concentration of about 5 mM the calibration curve deviates from the linear fit [28]. Higher concentrations can be determined by diluting the solution [28]. After adding excessive amounts of hydrogen peroxide to the ammonium metavanadate solution, the absorbance decreases and its colour changes to yellow [28].

The absorbance is maximal at a wavelength of 450 nm [28]. Therefore, the hydrogen peroxide concentration is calculated with the absorbance value at 450 nm. Throughout this work, the absorbance was computed as the logarithm of the basis 10:

$$A = -\log_{10}(I/I_0) \underset{\mathrm{Beer-Lambert}}{=} \epsilon l c \tag{3.6}$$

with the absorptivity ϵ, the length of the light path through a medium l and the concentration of the medium c according to the law of Beer-Lambert [35].

3.2.2 Setup

As shown in figure 3.4, a broadband laser driven light source (LDLS, Energetiq) is utilized for absorption spectroscopy. The LDLS covers a spectrum from 170 nm to 2500 nm. It was always turned on at least 20 min prior to experiments for stabilization. Following the path of the light from the source, lens 1 parallelizes the light before it hits the slit. The slit is adjusted in a way that the beam covers an area of $1\,\mathrm{mm} \times 6\,\mathrm{mm}$ on a UV-cuvette (Sarstedt polystyrene). The cuvette itself is fixed on a xz-stage using a 3d printed mount. After the light traverses the liquid, lens 2

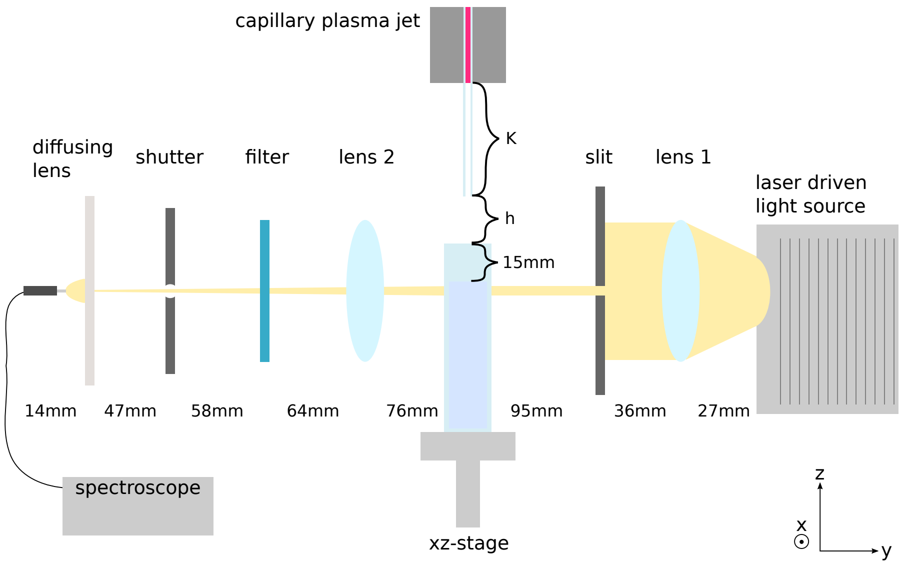

Figure 3.4: Sketch of the setup for the spectrophotometric approach.

collects it and focuses it through a filter with peak transmittance around 500 nm on a diffusing lens. The filter was necessary to prevent saturation of the spectrometer and maximise the signal at 450 nm. In figure 3.5 (left) the influence of the filter on the spectrum can be seen. Towards wavelengths in the ultraviolet or infrared regime hardly any light is transmitted. The diffusing lens is used to avoid notable changes in the intensity of the light caused by changes in the refraction index, which move the focus point slightly. An optical fibre couples the light into a spectroscope (Avantes Avaspec-ULS 2049x64 TEC-EVO). A mechanical shutter facilitates the saving of dark spectra.

The spectroscope is controlled and the spectra are saved with the software `Avasoft` (version 8.11.0.0) provided by Avantes. Before each measurement the reference spectrum for the given sample was saved. Thus, sample differences prior to adding hydrogen peroxide are accounted for. During the plasma treatment, spectra are saved periodically, which results in a spatially local and time dependent hydrogen peroxide concentration. Afterwards, a spectrum of the stirred solution is captured. Hereby, the average concentration in the liquid can be determined.

To conduct plasma treatment with this setup, a cuvette with the ammonium metavandate solution is placed in its mount and the reference spectrum is taken. Then the housing of the jet is lowered until the capillary levels with the upper edge of the cuvette. This refers to $h = 0$ mm (see figure 3.4). The distance between the plasma and the end of the capillary is denoted as K. The distance between liquid surface and tip of the cuvette amounts to 15 mm. The plasma is ignited and the power is continuously readjusted according to the power measurements. The built in timer function of the generator is utilised, to ensure accurate treatment times (mostly 5 min).

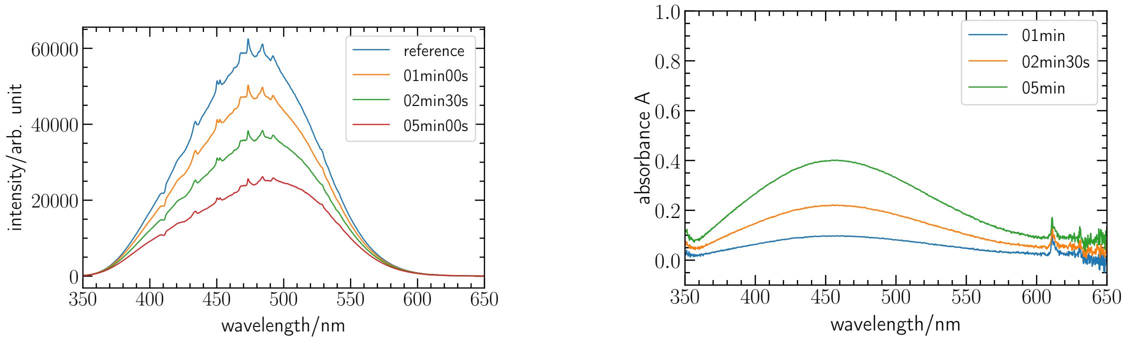

Figure 3.5: Example for the decreasing intensity of the spectra (left) and the absorbance (right) for several times during the plasma treatment which lasted 5 min.

In figure 3.5 the decreasing intensity and the increasing absorbance during plasma treatment are shown. The peak of the absorbance is indeed at approximately 450 nm.

3.2.3 Calibration and measurement uncertainties

In the following, the process of calibrating the spectrophotometric method is described and measurement uncertainties are discussed. In advance, the ammonium metavanadate solution is stirred magnetically for a couple of minutes to ensure the solution is homogeneous. A volume of 3 mL is filled to each cuvette using a pipette (Eppendorf 1 mL). For each sample a different reference spectrum is saved and afterwards a hydrogen peroxide reference solution is added to the sample. The reference solutions were prepared with 30 % hydrogen peroxide solution (Fisher Chemical). The liquid is stirred and a spectrum is saved. During this thesis two ammonium metavandate solutions were produced. For each solution a calibration was conducted and linear fits with the intercept preset to zero were calculated:

- 27.01.2022: $A = (0.29 \pm 0.01)c$, $R^2 = 0.98876$
- 22.02.2022: $A = (0.300 \pm 0.003)c$, $R^2 = 0.99720$

with the absorbance A and the hydrogen peroxide concentration c. For the calibration on 27th January 2022, half a litre of ammonium metavanadate solution was prepared. The slopes of both linear fits are similar, which indicates the reproducibility of the method. In figure 3.6 the calibration for 22nd February 2022 is shown because the measurements were conducted with this ammonium metavanadate solution. The aforementioned saturation at hydrogen peroxide concentrations of approximately 5 mM (see section 3.2.1) can be observed in figure 3.6 as well.

To investigate the measurement uncertainty of the method, the hydrogen peroxide concentration utilizing two reference concentrations was determined for five samples. In figure 3.7 (left) the calculated hydrogen peroxide concentration, the observed

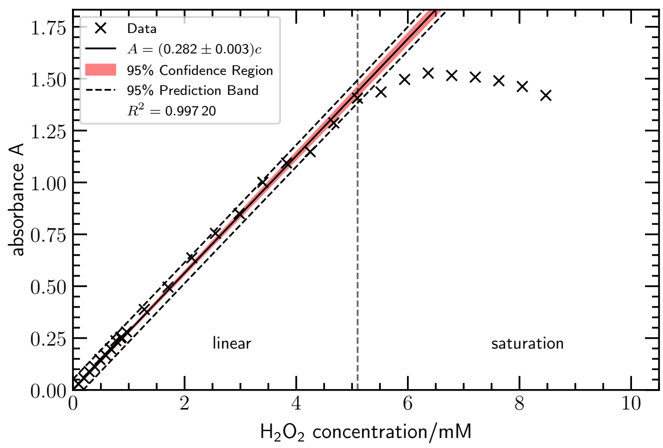

Figure 3.6: Calibration of the spectrophotometric method (22.02.2022). The absorbance as function of the hydrogen peroxide concentration is displayed.

hydrogen peroxide concentrations and the mean are plotted for each sample. The coloured area depicts the standard deviation around the mean. The observed concentrations are higher than the calculated ones. This could be to due to a systematic error. Possibly the volume dispatched into the sample with the cuvette varied. Because it is not clear if the systematic error is caused by the diagnostic or the reference concentration and by reason of its magnitude it is neglected. As measurement uncertainty the higher relative error of both concentrations 4 % is chosen.

A second measurement uncertainty is given by the plasma treatment (see figure 4.8), right). Two different scenarios were analysed: repeated plasma treatment with constant parameters (no. 1 to 5) and readjusting the position of the electrodes between measurements (no. 6 to 10 and 11 to 13). Measurements 11 to 13 were conducted five days after the previous ones. The liquid was treated for 5 min at a power of 6 W, a water concentration in the gas flow of (6700 ± 300) ppm and helium as working gas. If not indicated otherwise, all the results were obtained with a distance between plasma and the end of the capillary of (8.0 ± 0.5) mm and the end of the capillary levelling with the top of the cuvette ($h = (0.0 \pm 0.5)$ mm). The average concentrations after stirring the liquid were taken.

In sum, the plasma treatment without readjusting the jet shows a relative error of 1 %. Therefore, the relative error derived from the calculated hydrogen peroxide concentration is used for error bars, in the case that the jet was not readjusted between measurements. If the jet is readjusted, the hydrogen peroxide concentration varies significantly. The concentrations can be related to the position of maximum emission of the plasma as shown in figure 3.8. It seems that electrode adjustments with the maximum plasma emission in the lower part of the capillary lead to higher hydrogen peroxide concentrations (e. g. no. 8 and 12). A possible explanation could be the shorter distance between liquid and the lower part of the capillary yielding

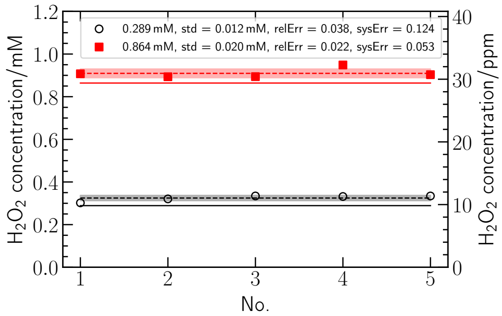

Figure 3.7: Measurement uncertainty for the spectrophotometric method. The uncertainty of the method was analysed with reference solutions (left) and the uncertainty according to the plasma treatment was determined (right).

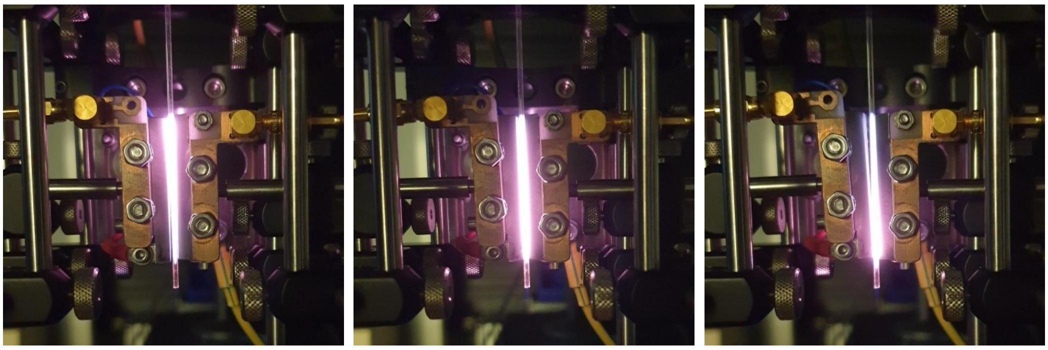

Figure 3.8: Photographs of the plasma emission for different electrode adjustments. The plasma is brighter in the upper (left) or lower (right) part of the capillary. Additionally, the plasma can emit light homogeneously (middle).

fewer hydrogen peroxide losses on its pathway. The relative error of 16 % due to readjusting the jet is utilized for error bars in case the jet was readjusted between measurements.

3.3 Electrochemical approach

Additionally to the spectrophotometric approach, a second diagnostic is applied to verify the results. It is based on the electrocatalytic reaction between Prussian blue and hydrogen peroxide [22].

3.3.1 Concept and setup

The aforementioned electrocatalytic reaction converts hydrogen peroxide and two electrons to two hydroxide ions:

$$H_2O_2 + 2\,e^- \xrightarrow{k_{cat}} 2\,OH^- \tag{3.7}$$

with the bimolecular rate constant $k_{cat} = 3 \times 10^3\,M^{-1}\,s$ [22]. The device consists of a reference electrode, a counter electrode and an electrode with a layer of Prussian blue. Prussian blue is also called ferric ferrocyanide ($Fe_4{}^{III}[Fe^{II}(CN)_6]_3$) and consists of iron ions coordinated to carbon and nitrogen respectively [21]. During the 60 s long measurement, a potential is applied between the electrodes and the current is measured. The peak current is linearly dependent on the hydrogen peroxide concentration in the solution [22]. Karyakin and Karyakina calibrated their electrode for hydrogen peroxide concentrations between 0.1 µM and 0.1 mM [22]. In a more recent work of Yang et al. a detection range from 50 µM to 11.3 mM was achieved [42]. The electrochemical method should be applicable to the plasma treated solutions, because the expected hydrogen peroxide concentration lies in the millimolar range.

Regarding the setup, the utilized probe was assembled by colleagues in the department for electrochemistry (Tschulik) of the Ruhr-Universität Bochum. As liquid a ph buffer solution (K_2HPO_4 38.7 mM; KH_2PO_4 61.3 mM; ph7) designed for the enzymes (chair for applied microbiology, Bandow) was used. Due to the lack of equipment, the ph value of the solution was not adjusted before each measurement. To conduct a measurement, the sample is decanted from the cuvette to a beaker. Then the electrochemical probe is placed inside the solution as illustrated in figure 3.9 and connected to an electrochemical interface by PalmSense. This can be operated via a computer using the software `PSTrace` (version 5.9.2317) provided by PalmSense. `PSTrace` is set to the technique 'chronoamperometry' with the default settings ($t_{equilibration} = 8\,s$, $U_{DC} = -0.1\,V$, $t_{interval} = 0.1\,s$).

In contrast to the spectrophotometric approach, the electrochemical probe measures only the average hydrogen peroxide concentration after the plasma treatment.

3.3.2 Calibration and measurement uncertainties

The procedure is similar to the calibration of the spectrophotometric approach with ammonium metavanadate. Ten different hydrogen peroxide concentrations from 0.097 mM to 0.960 mM were prepared. Using the cuvettes as vessel resulted in abrasion of the electrodes. Therefore, the housing for the electrochemical probe was changed. In figure 3.10 the two different housings are shown. For each housing a separate calibration was performed. The electrochemical probe was placed in the housing on the left hand side during the second calibration and all the following measurements.

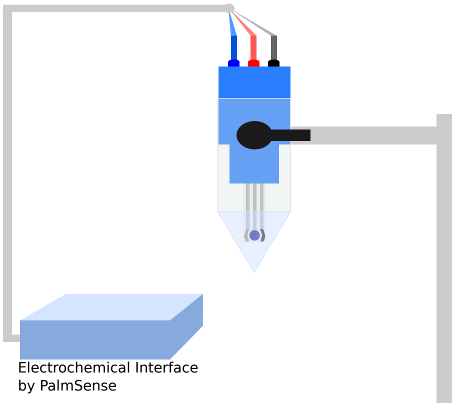

Figure 3.9: Sketch of the setup for the electrochemical approach.

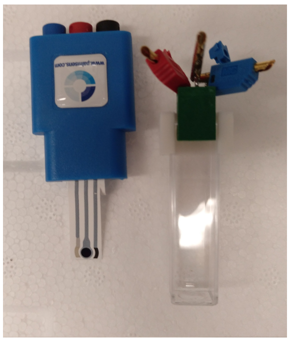

Figure 3.10: Two housings for the electrochemical probe. The housing on the left hand side was used in the measurements.

All solutions were stirred before the measurements to ensure the hydrogen peroxide concentration is homogeneously distributed. In the second calibration stirring was not necessary because the solution was decanted from the cuvette in a different vessel.

- 18.03.2022: $I = (-3.7 \pm 0.1)c$, $R^2 = 0.976\,07$
- 22.03.2022: $I = (-3.8 \pm 0.1)c$, $R^2 = 0.989\,29$

Both linear fits with the intercept preset to zero are pictured in figure 3.11. The second calibration as shown in figure 3.11 (right) exhibits less fluctuations in the measured current. In the first calibration the current does not decrease further for concentrations above 0.8 mM (see figure 3.11, left) which could not be reproduced in the second calibration. Thus, it is probably due to worse contact with the electrodes, because of the aforementioned abrasion. In both cases, the measurement at 0.093 mM does not match the other ones. As the indicated problem kept occurring for the first measurement in a series and the temporal course of the current (not shown) did not match the other measurements, two measurements in the buffer solution without hydrogen peroxide were conducted prior to each measurement series to clean the surface of the electrodes.

Analogous to the procedure in section 3.2.3 the measurement uncertainty was investigated. In figure 3.12 (left) the calculated hydrogen peroxide concentration as well as the observed concentrations are plotted. The observed concentrations are about 30 % below the calculated ones. Therefore a systematic error in the method has to exist. A third calibration was performed yielding a significantly different linear fit:

- 11.04.2022: $I = (-1.9 \pm 0.1)c, R^2 = 0.803\,164$

Calculating the concentration for the same peak currents with the new calibration leads to higher observed than calculated concentrations (see figure 3.12, right). This results support the assumption that the electrochemical probe is not working properly and needs to be replaced. Regarding the measurements, this means that absolute values are not correct, but the trends should be displayed properly. As uncertainty for one measurement series, a relative error of 5 % is utilized.

3.4 Evaporation of the liquid

The evaporation of the liquid due to the plasma treatment was measured by weighing the cuvette and the liquid with a high precision scale (Radwag As X2 PLUS) prior to and after the treatment. The evaporation could only be calculated for the spectrophotometric measurements due to the decanting of the liquid for the electrochemical measurements (see section 3.3). From the mass difference a volume was determined. Hereby, the density of water ($1\,\mathrm{kg\,m^{-3}}$) approximates the density of the liquid. This approximation should be accurate due to the high dilution of the ammonium metavanadate and the sulphuric acid (see section 3.2). The evaporation amounts to about 0.1 mL (3.3 % of the total volume) for a treatment time of 5 min at a power of 6 W and a water concentration in the gas flow of (6700 ± 300) ppm. This causes a decrease of the liquid level in the cuvette of about 1 mm.

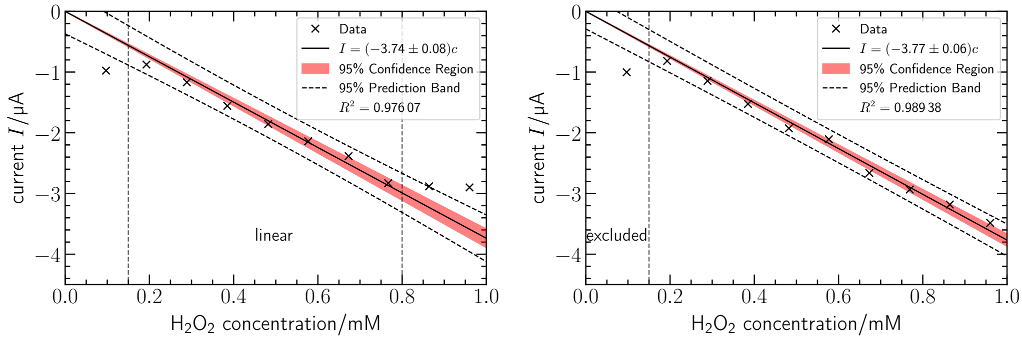

Figure 3.11: Two calibrations of the electrochemical method were performed. The calibration from 18.03.2022 corresponds to the old housing (left) and the calibration from 22.03.2022 to the new housing (right).

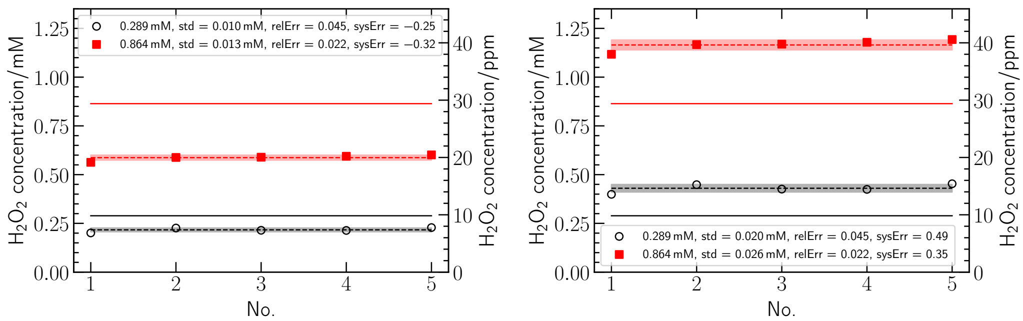

Figure 3.12: Measurement uncertainty for the electrochemical method. The observed concentrations were calculated for the old (left, 22.03.22) and the new calibration (right, 11.04.22).

4 Results and Discussion

In section 2.3 research questions and parameter variations were proposed. The results of these variations of dissipated power, water admixture, working gas, residence time and frequency modulation will be presented and discussed in the following. If not stated otherwise, the plasma treatment was conducted for 5 min, with a power of 6 W, at water concentrations of (6700 ± 300) ppm and a gas flow of 1 slm. Also the distance between the plasma and the end of the capillary K and the distance between the end of the capillary and the upper edge of the cuvette h (see figure 3.4) usually amounted to (8.0 ± 0.5) mm and (0.0 ± 0.5) mm. For the spectrophotometric method the average concentrations after stirring the solution are reported.

During the treatment the hydrogen peroxide is created in the plasma and is transported in the effluent to the liquid surface. As hydrogen peroxide is a long-lived species, it is assumed that the hydrogen peroxide generated in the plasma reaches the liquid surface. Due to its hydrophilic character [4] presumably all hydrogen peroxide molecules will be absorbed into the liquid. In the liquid the hydrogen peroxide is stabilized [4] and accumulates due to its long lifetime (see section 2.2). Thus, the dependency of the hydrogen peroxide concentration in the liquid on the aforementioned parameters can be transferred to the hydrogen peroxide concentration in the plasma. With the spectrophotometric method it is possible to determine the hydrogen peroxide concentration while treating the liquid with the plasma. Although these measurements only show the local concentration at the position where the light transverses the cuvette, it gives an insight into the temporal evolution of the hydrogen peroxide concentration in this region. In figure 4.1 the temporal evolution is shown. The measurements indicate that the hydrogen peroxide concentration increases linearly with time. This could be observed for treatment times up to 30 min (not shown). For the application the linear dependence is advantageous because the amount of hydrogen peroxide can be increased by treating the liquid for longer time periods.

4.1 Power dissipated in the plasma (RQ1)

In this section the relation between the power coupled into the plasma and the hydrogen peroxide concentration is thematised. Not only does the power influence the production and loss processes of hydrogen peroxide through the electron and gas

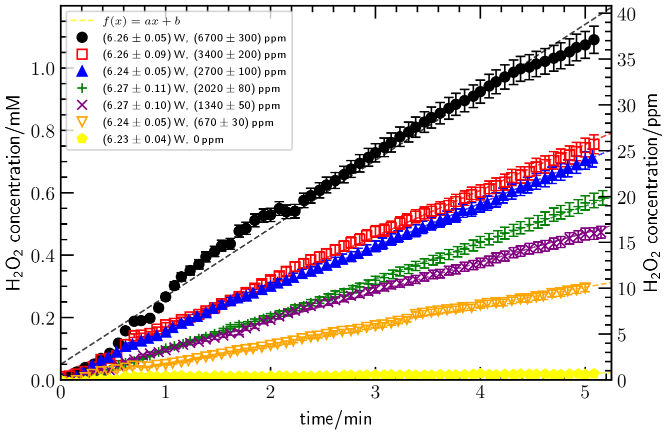

Figure 4.1: The hydrogen peroxide concentration as function of the time measured with the spectrophotometric method. As an example, the 6.2 W measurement of the power and water admixture variation for a total gas flow of 1 slm is shown.

temperature (see section 2.2), but it also changes heating processes in the discharge, which results in different operating regimes (see section 2.1). Vasko et al. found a linear dependency between hydrogen peroxide concentration and the power dissipated in the plasma for a similar setup (μ-APPJ without capillary and plasma volume of 175 m^3) [38]. In a different study Yayci et al. also reported a linear dependency using the COST-jet as plasma source [45]. To begin with, the hydrogen peroxide concentration as function of the power is shown in figure 4.2 for the small capillary. The power was varied between 0.8 W and 12 W for several water concentrations. The different symbols and colours in figure 4.2 correspond to these water concentrations in the gas flow. They were varied by changing the ratio between the gas flow through the bubbler system and the total gas flow (here 1 slm). Water vapour concentrations in the gas flow of up to (6700 ± 300) ppm were reached.

In figure 4.2 (left) the hydrogen peroxide concentration on the y- (left: mM, right: ppm) and the power dissipated in the plasma on the x-axis are displayed. The hydrogen peroxide concentration increases with the power. However, it stagnates for powers of 6 W and higher. A maximal hydrogen peroxide concentration of 0.95 mM (32 ppm) was obtained for a power of about 6 W and a water concentration of (6700 ± 300) ppm. Additionally, it can be seen that more hydrogen peroxide is produced when the water concentration in the gas flow is increased. The effects of the water concentration are discussed more detailed in section 4.2. To validate the results of the spectrophotometric method, the measurements were conducted with the electrochemical approach as well. For the latter, similar trends are observed (see figure 4.2, right). The absolute values of the hydrogen peroxide concentration determined with the electrochemical probe are lesser than the ones measured with the spectrophotometric approach. This was expected because of the degradation issues with the electrochemical probe (see section 3.3.2).

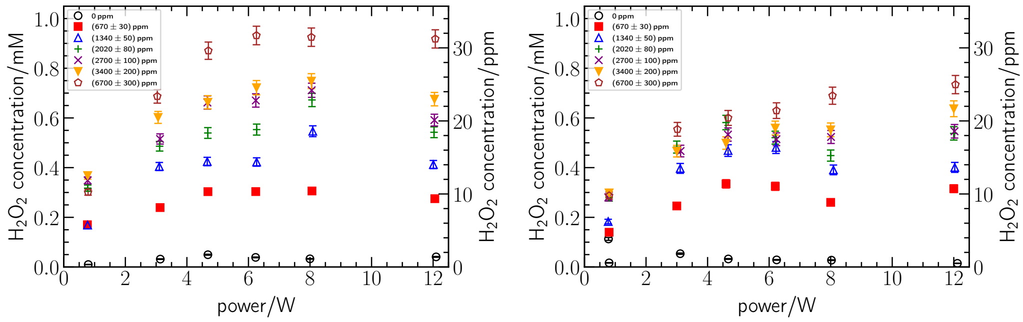

Figure 4.2: Hydrogen peroxide concentration as function of the power coupled into the plasma for several water concentrations in the gas flow for the small capillary. The hydrogen peroxide concentration was determined with the spectrophotometric (left) and the electrochemical method (right). All hydrogen peroxide concentrations are averages of the whole volume observed after 5 min treatment time and the total gas flow amounted to 1 slm.

To validate the aforementioned results, they are compared with investigations of other groups. Vasko et al. reported a linearly increasing hydrogen peroxide concentration for powers up to 2.75 W at a water concentration of 6000 ppm [38]. Likewise Yayci et al. reported a linear increase with voltage as the power was not measured [45]. These results are in agreement with the data in figure 4.2.

In the following, explanations for the observed trends are hypothesized. The increasing hydrogen peroxide concentration at lower powers could be due to more dissociation of water molecules as this process depends on the electron density and the dissociation rate coefficient increases with electron temperature (see equation (2.7)). The more water is dissociated the more hydroxyl is generated and can then associate to hydrogen peroxide. A possible reason for the saturating hydrogen peroxide concentration in figure 4.2 could be the gas temperature increase with power. On the one hand, the rate coefficient for hydrogen peroxide production (see equation (2.5)) decreases with the gas temperature ($\propto (T_{\mathrm{gas}}/300)^{-0.8}$). On the other hand, the rate coefficient of the main loss process (see equation (2.6)) increases with the gas temperature ($\propto \exp(-1/T_{\mathrm{gas}})$). Considering both processes, the saturation of the hydrogen peroxide concentration could be attributed to the increasing gas temperature. Effluent temperature measurements with the thermocouple were not accurate and thus cannot validate that hypothesis. In figure 4.3, which was taken from Winzer et al., the gas temperature as function of the power at a constant admixture of 0.5 % O_2 is shown. Although molecular oxygen is added to the gas instead of water vapour, the increase of the temperature with power should be comparable. This would support the hypothesis that increasing gas temperatures cause the stagnation of the hydrogen peroxide concentration.

In addition to the small capillary, the same measurement series was conducted for the wide capillary and two distinct water admixtures ((1340 ± 50) ppm and

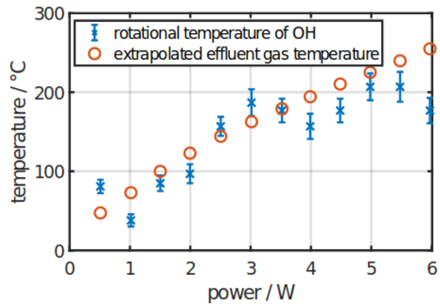

Figure 4.3: Gas temperature in the plasma extrapolated from the effluent compared to the rotational temperature from the A-X transition of the OH-radical as a function of the dissipated power at constant admixture of 0.5 % O_2. Figure taken from Winzer et al. [41].

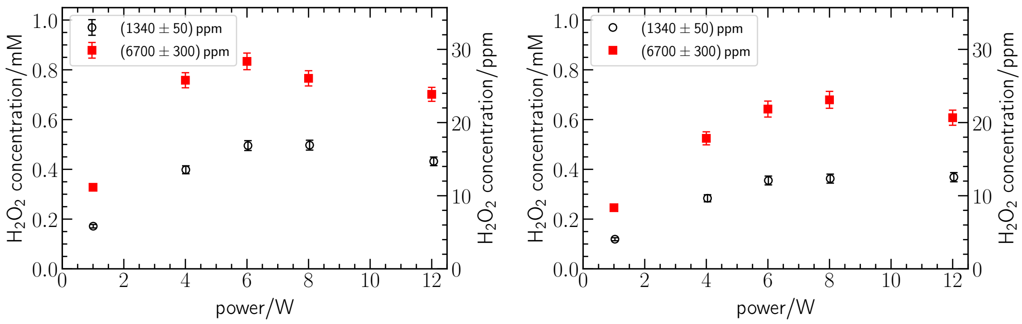

Figure 4.4: Hydrogen peroxide concentration as function of the power coupled into the plasma for several water concentrations in the gas flow for the wide capillary. The hydrogen peroxide concentration was determined with the spectrophotometric (left) and the electrochemical method (right). All hydrogen peroxide concentrations are averages of the whole volume observed after 5 min treatment time and the total gas flow amounted to 1 slm.

(6700 ± 300) ppm). Comparing results between the two capillaries, the higher cross section of the wide capillary needs to be considered. Therefore, the velocity towards the liquid and by this the flux of hydrogen peroxide molecules on the liquid surface are different for the small and the wide capillary. Additionally, the residence time differs. Thus, the absolute hydrogen peroxide concentrations are not comparable for the measurements described here. Hence, the dependency of the hydrogen peroxide concentration on the power is compared in the following. This is displayed in figure 4.4. The wide capillary exhibits a maximal hydrogen peroxide concentration of about 0.85 mM around a power of 6 W and for a water concentration of (6700 ± 300) ppm. The hydrogen peroxide increases with power up to 6 W. For higher powers, it decreases slightly. Increasing the water concentration in the gas flow leads to higher hydrogen peroxide concentrations in the liquid. Both trends are supported by the measurements conducted with the electrochemical probe (see figure 4.4, right). Thereby, the dependency of the hydrogen peroxide concentration on the power as well as water admixture is comparable for both capillaries. Nonetheless, the different hydrogen peroxide fluxes or residence times probably cause the dissimilar absolute hydrogen peroxide concentrations.

4.2 Water admixture (RQ2)

The water concentration in the gas flow influences the hydrogen peroxide concentration by the amount of water molecules which can contribute to the hydrogen peroxide production. As deduced in section 2.2, in zero order approximation and neglecting loss processes two water molecules are needed to produce one hydrogen peroxide molecule. This suggests a linear relation between the water and the hydrogen peroxide concentration.

To give a better overview regarding the relation between hydrogen peroxide concentration and water admixture, in figure 4.5 (left) the hydrogen peroxide concentration for the small capillary is shown as function of the water concentration. The data is the same as used for the left graph of figure 4.2. If no water vapour is added to the gas flow, the hydrogen peroxide concentration is close to zero (< 0.05 mM). It was expected that the hydrogen peroxide is exactly zero. However, the difference is probably due to rest humidity in the gas system. Furthermore, the hydrogen peroxide concentration in the liquid increases quickly at lower water concentrations. Then the corresponding slope decreases and almost saturates. This is not in agreement with the results from Vasko et al., as they report a linear relation for water concentrations up to 10 000 ppm [38]. Nevertheless, simulation and experimental results obtained by Schröter show a non-linear relation, which matches the trend in figure 4.5 (left). Schröter utilised a modified, sealed version of the COST-jet [31] and thus the setup is comparable. As possible reasons for the deviation from a linear correlation, Vasko et al. hypothesized the role of hydroxyl (OH) in the destruction of hydrogen peroxide (see section 2.2) as well as the changes in electron density and temperature [38]. The hydroxyl density in the gas phase was investigated by Benedikt et al. [2]. Utilising a plasma source resembling the COST-jet, they found the same trend as seen in figure 4.5 (left) but for the hydroxyl density in the gas [2]. This is in agreement with the trend seen in figure 4.5 (left) and the measurements by Schröter, as the hydroxyl density is linked to the hydrogen peroxide concentration by the aforementioned production and loss processes. It has to be mentioned that complete saturation did not occur in the investigated measurement range (see figure 4.5, left). Only for a power of 0.8 W a local maximum (about 0.35 mM) can be found at a water concentration around (3400 ± 200) ppm. Possibly this power is not sufficient to support the reactions in the plasma (see section 2.2), e. g. resulting in lower electron temperature. By the latter, the dissociation of water molecules is decreased (see equation (2.7)) and thus could cause lower hydrogen peroxide concentrations.

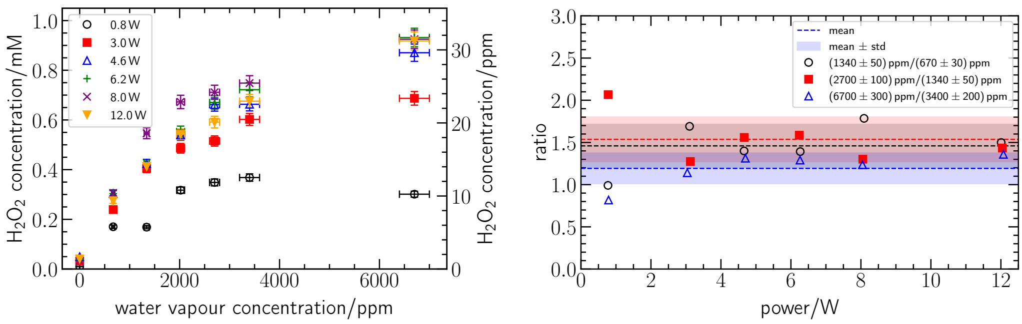

Figure 4.5: Hydrogen peroxide concentration as function of the water admixture for the small capillary (left) obtained with the spectrophotometric method. The ratio of the hydrogen peroxide concentration for different pairs of water admixtures was plotted for several powers (right). All hydrogen peroxide concentrations are averages of the whole volume observed after 5 min treatment time and the total gas flow amounted to 1 slm.

To analyse the importance of hydrogen peroxide loss processes and the expected linear relation between the hydrogen peroxide and the water concentration, ratios of the hydrogen peroxide concentration were calculated. As deduced at the start of this section, the dependence of the hydrogen peroxide concentration on the water concentration is expected to be linear. In figure 4.5 (right) the ratio of the hydrogen peroxide concentrations for pairs of water vapour concentrations is shown. The pairs are chosen so that the water concentration is two times higher for each pair. If the relation is linear, the ratios should equal 2. The loss processes neglected in this approximation as well as changes in electron density and temperature could cause the lower observed ratio of 1.5. The ratios for a power of 0.8 W deviate significantly from the mean. This can be explained by the corresponding trend of the hydrogen peroxide concentration as seen in figure 4.5 (left). It contains a local maximum which causes the ratio to drop below 1. Additionally, there is a plateau at a water concentration of (1340 ± 50) ppm which accounts for the ratio above 2.

In sum, the ratio of 1.5 indicates that the aforementioned loss processes play an important role and that the relation between the hydrogen peroxide concentration and the water concentration is non-linear. For higher water concentrations (△, blue; (6700 ± 300) ppm/(3400 ± 200) ppm), the mean of the ratio lies at 1.2, which indicates that the loss processes are even more important in this regime.

4.3 Working gas (RQ3)

One important control parameter of the plasma source is the working gas. It changes the characteristics of the discharge, e. g. electron temperature and density as well as the gas temperature (see section 2.1). This influences the hydrogen peroxide concentration by the rate coefficients regarding hydrogen peroxide production and loss processes (see section 2.2). For other plasma sources, the use of argon was beneficial for the hydrogen peroxide production [38]. In the previous sections 4.1 and 4.2 helium was used as working gas. To compare the performance of helium and argon, the hydrogen peroxide concentration was measured for an argon discharge at several powers and water admixtures. The corresponding results are described in the following.

In figure 4.6 the observed hydrogen peroxide concentrations as function of the power can be seen. To compare argon with helium, the hydrogen peroxide concentration for the helium discharge at a power of 6 W and a water concentration of (3400 ± 200) ppm was added (∇, yellow). Its uncertainty corresponds to the deviation due to adjusting the jet shown in figure 3.7 (right). With this setup, the use of argon as working gas yields lower hydrogen peroxide concentrations than the use of helium as working gas (see figure 4.6). The maximal hydrogen peroxide concentration achieved with argon was about 0.4 mM after 5 min treatment time and at a power of 20 W. The water concentration could not be increased further as the discharge did not ignite. However, with helium a hydrogen peroxide concentrations of about 0.75 mM was obtained for the same water admixture and at a lower power of 6 W. Thereby, the use of helium as working gas yields higher hydrogen peroxide concentrations and is more efficient.

In addition to lower hydrogen peroxide concentrations, using argon resulted in unstable working conditions. For example, the power increased strongly with time during the measurement. However, it could not be decreased by adjusting the voltage, because then the discharge extinguished. This is most likely due to heating effects, which is supported by the lower thermal conductivity of argon compared to helium (see section 2.1). Especially for the 20 W measurement, the jet and the effluent were heating up considerably. As mentioned before, the measurement of the effluent temperature with a thermocouple proved to be not accurate with fluctuations of about 30 °C. Nevertheless, a gas temperature in the effluent around 300 °C was observed at a power of 20 W. Finally, we decided to use helium as working gas for

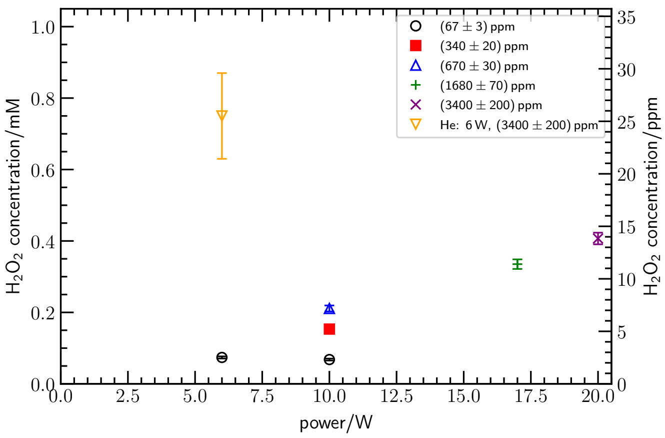

Figure 4.6: Hydrogen peroxide concentration with argon as working gas for different power and water admixtures. The average hydrogen peroxide concentrations obtained with the spectrophotometric method after 5 min treatment time and with a total gas flow of 1 slm are used.

further measurements because of the higher hydrogen peroxide concentrations and its better handling.

Generally, the better performance of helium contradicts the expectation formulated above and in section 2.3. The problems regarding the ignition of the argon discharge can be explained by the Paschen curve mentioned in section 2.1. However, the reason for the lower hydrogen peroxide concentration in the argon discharge is not clear. A possible explanation could be the gas temperature dependency on the rate coefficients or a lower electron temperature. The latter results in less dissociation of water molecules by electrons. Being the main hydroxyl (OH) source (see equation (2.7)), less dissociation of water interferes with hydrogen peroxide production as hydroxyl yields hydrogen peroxide in a three body association (see equation (2.5)). Therefore, a lower electron temperature in the argon discharge [10] could explain the worse performance regarding the hydrogen peroxide production. Also the hydrogen peroxide should decrease for increasing gas temperatures.

4.4 Residence time (RQ4)

Additionally to the power and water admixture, the residence time of the species was investigated. Due to findings of Vasko et al., the hydrogen peroxide concentration is expected to increase towards shorter residence times [38]. In doing so, the total gas flow was varied. However, a variation of the total gas flow changes not only the residence time in the plasma, but also the travel time in the capillary after leaving the plasma and the travel time in the atmosphere. Therefore, the influence of these times on the hydrogen peroxide concentration is analysed additionally. Moreover, a higher gas flow results in a higher flux of hydrogen peroxide particles on the liquid surface. In the following, results of the total gas flow variation are discussed.

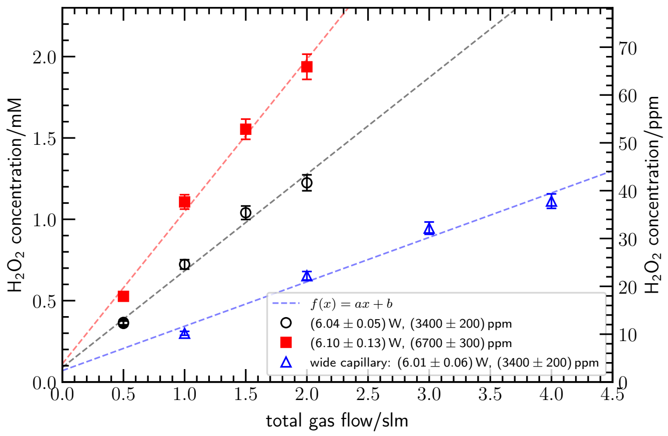

Figure 4.7: Hydrogen peroxide concentration depending on the total gas flow for both capillaries with the indicated water admixtures at a power of about 6 W. The average hydrogen peroxide concentrations obtained with the spectrophotometric method after 5 min treatment time are used.

In figure 4.7 the relation between the hydrogen peroxide concentration and the total gas flow is shown. As can be seen, the hydrogen peroxide concentration increases linearly with the total gas flow. For the small capillary and a water concentration of (6700 ± 300) ppm the slope roughly amounts to $1\,\mathrm{mM\,slm^{-1}}$. Furthermore, a maximal hydrogen peroxide concentration of about 2 mM is observed for the same measurement series. With a similar setup using the COST-jet as plasma source, Yayci et al. reported a hydrogen peroxide production rate of about $320\,\mathrm{nmol\,min^{-1}}$ for a total gas flow of 1.4 slm, 20 % flow through the bubbler system at room temperature and a peak to peak voltage of 330 V [45]. In general, a comparison of two plasma sources, in this case COST-jet and capillary jet, is difficult as many parameters need to be considered. Nevertheless, the production rate for the maximal concentration of 2 mM obtained with the capillary jet amounts to $1200\,\mathrm{nmol\,min^{-1}}$. This is about four times higher than the production rate with the COST-jet. Thereby, the capillary jet seems to be more suitable for the project B11.

Because the variation of the total gas flow changes residence as well as travel time, additional measurements were conducted. In doing so, the distance between the plasma and the end of the capillary K (see figure 3.4) was varied. In all of these measurements the capillary levelled with the top of the cuvette ($h = 0$). In figure 4.8 (left) the hydrogen peroxide concentration as function of the distance between plasma and liquid surface is shown. The hydrogen peroxide concentration decreases linearly, if the plasma is further away from the end of the capillary. This is in agreement with observations by Schröter, which were obtained with a comparable setup [31]. Moreover, the relation between distance K and hydrogen peroxide is weaker than its

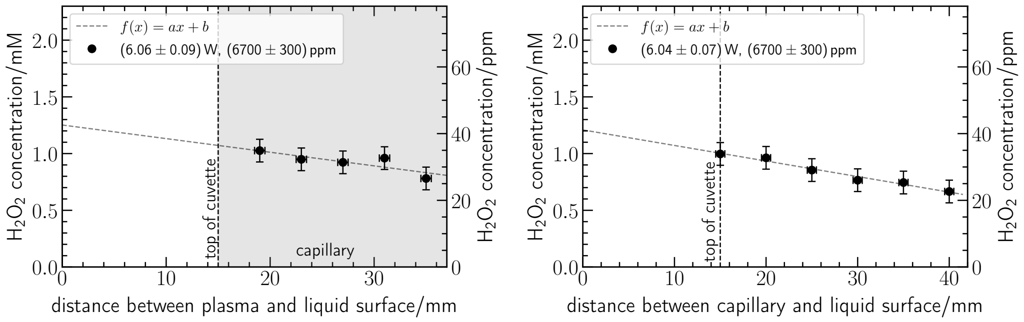

Figure 4.8: Hydrogen peroxide concentration as function of the distance between plasma and liquid surface (left) as well as the distance between capillary and liquid surface (right) for the small capillary. In both figures the liquid surface is located at 0 mm. The distances change the travel time in the capillary (left) and the travel time in the atmosphere (right) respectively. The average hydrogen peroxide concentrations obtained with the spectrophotometric method after 5 min treatment time and with a total gas flow of 1 slm are used.

dependence on the total gas flow. For example, doubling the total gas flow increases the hydrogen peroxide concentration by a factor 2 (see figure 4.7). On the other hand, doubling the distance K, which also changes the travel time in the capillary along K by a factor 0.5, the hydrogen peroxide concentration does not decrease by a factor 2. Thus, the travel time in the capillary along K plays a minor role for the observed hydrogen peroxide concentration.

Additionally, the total gas flow influences the time the species move through the atmosphere. To vary this travel time, the distance between the end of the capillary and the tip of the cuvette, denoted as h (see figure 3.4), was controlled. Moreover, the distance between the tip of the cuvette and the liquid surface amounted to 15 mm. Hereby, the distance changes by evaporation are neglected. The variation of the distance between capillary and liquid surface was conducted and the resulting hydrogen peroxide concentrations are shown in figure 4.8 (right). The hydrogen peroxide concentration decreases linearly with the aforementioned distance. To prove if the trend observed in figure 4.7 can be attributed to the distance variation, two distances in figure 4.8 (right) are compared. This yields that doubling the distance does not halve the hydrogen peroxide concentration. For example, at a distance of 15 mm the hydrogen peroxide concentration amounts to about 1 mM and at 30 mm it is about 0.75 mM. Hence, for this distance variation the slope is lower than the one observed for the total gas flow variation. Therefore, the distance between capillary and liquid surface and by this the travel time in the atmosphere do not influence the hydrogen peroxide concentration as strongly as the variation of the total gas flow.

In sum, the travel time in the capillary after the plasma and the travel time in the atmosphere do not influence the hydrogen peroxide concentrations greatly. Considering the changes in hydrogen peroxide concentrations, the variation of the total gas flow approximately reflects the variation of the residence time in the plasma. However, also the flux of hydrogen peroxide molecules is varied. The dependency of the hydrogen peroxide concentration on the residence time and the particle flux will be discussed later on. From the data in figure 4.7 residence times in the plasma were calculated by assuming a constant and laminar gas flow. The length of the plasma amounts to 40 mm. The hydrogen peroxide concentration as function of the residence time is presented in figure 4.9 (left). Firstly, the measurements agree well with the fits ($f(x) = a + b/x$). This is due to the transformation from total gas flow to residence time because the time depends on the inverse of the total gas flow ($t = s/v = sA/\phi_{\text{total}}$ with the plasma length s, the velocity v, the cross section A and the total gas flow ϕ_{total}). In figure 4.9 (left) the two capillaries are comparable because in the calculation of the residence time the different cross sections are accounted for. The wide capillary (△, blue) has to be compared to the small capillary with the same water concentration in the gas flow (○, black). The comparison between small and wide capillary for a residence time of 2.4 ms shows, that the wide capillary produces more hydrogen peroxide, 1.1 mM (wide) compared to 0.6 mM (small). Its hydrogen peroxide concentrations are even slightly higher than the ones of the small capillary with double the water concentration.

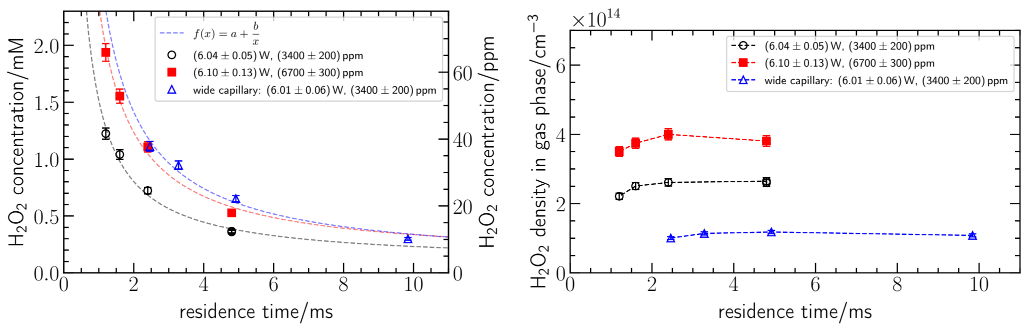

Figure 4.9: Hydrogen peroxide concentration in the liquid (left) and hydrogen peroxide density in the gas phase (right) depending on the residence time in the plasma for both capillaries. The average hydrogen peroxide concentrations obtained with the spectrophotometric method after 5 min treatment time are used.

As stated above, both the flux of hydrogen peroxide particles and the residence time change with the total gas flow. If the residence time caused the aforementioned changes, the hydrogen peroxide density in the plasma volume would have increased towards short residence time as seen for the hydrogen peroxide concentration in figure 4.9 (left). Nevertheless, the hydrogen peroxide concentration displayed in figure 4.9 still depends on the flux. Therefore, the dependence on the hydrogen peroxide flux is investigated in the following. Considering two approximations, the hydrogen peroxide density in the gas phase can be calculated from the concentration in the liquid. First, loss processes on the pathway to the liquid surface are neglected. Moreover, due the hydrophilic character of hydrogen peroxide, all hydrogen peroxide molecules in the gas phase above the liquid surface are absorbed. Then the number of hydrogen peroxide molecules in the liquid equals its pendant generated in the plasma. To calculate the number of hydrogen peroxide particles $N_{H_2O_2}$ from the concentration $c_{H_2O_2}$ (in mM = mol L^{-1}), the latter is multiplied by the liquid volume V_{liq} (3 mL) and the Avogadro constant N_A. By considering the units it is validated that the computation yields the number of particles:

$$[c_{H_2O_2}] \times [V_{liq}] \times [N_A] = 1 \times 10^{-3} \frac{\text{mol}}{\text{L}} \times \text{mL} \times \text{mol}^{-1} = 1 \times 10^{-6} \tag{4.1}$$

Furthermore, the flux of hydrogen peroxide particles, which describes the number of particles per volume and per time, can be described by

$$\Gamma_{H_2O_2} = \frac{N_{H_2O_2}}{V t_{treat}} \underset{V=\phi_{total} t_{treat}}{=} \frac{N_{H_2O_2}}{\phi_{total} t_{treat}^2} \overset{*}{=} \frac{n_{H_2O_2}}{t_{treat}} \tag{4.2}$$

with the total gas flow ϕ_{total}, the number density $n_{H_2O_2}$ and the treatment time t_{treat}. Combining both relations and solving the equation ($*$) for the density yields

$$n_{H_2O_2} = \frac{c_{H_2O_2}[\text{mM}] V_{liq} N_A}{\phi_{total} t_{treat}} \tag{4.3}$$

where $c_{H_2O_2}[\text{mM}]$ is the concentration in mM. In figure 4.9 (right) the hydrogen peroxide density in the gas phase is shown as function of the residence time. As the density in the gas phase does not depend on the flux, the impact of the residence time can be seen. The density hardly changes with residence time and is not increasing towards short residence times. However, a trend with a local maximum can be seen for the three curves. For the wide capillary the hydrogen peroxide density in the gas phase is lower than for the small capillary. This is due to its higher cross section (see equation (4.3)). Because of the weak dependency of the hydrogen peroxide density on the residence time, it should not influence the hydrogen peroxide concentration in the liquid strongly. Thereby, the increase in concentration as seen in figure 4.7 and 4.9 can be attributed to the increasing particle flux on the liquid surface.

In sum, the total gas flow, distances, the residence time and the particle flux were investigated. On the one hand, the variation of the distances does not affect the hydrogen peroxide concentration strongly. On the other hand, the calculation of residence times yields that the wide capillary produces more hydrogen peroxide than the small one. An explanation could be that it is slightly wider than the electrodes (see section 3.1). Therefore, gas is flowing alongside of the plasma causing fewer hydrogen peroxide losses at the walls. Another difference is the higher volume to surface ratio of the wide capillary:

- small capillary: $40\,\text{mm}^3/(4 \times 40\,\text{mm}^2) = 0.25\,\text{mm}$
- wide capillary: $165.6\,\text{mm}^3/(2 \times 156\,\text{mm}^2 + 2 \times 36\,\text{mm}^2) \approx 0.43\,\text{mm}$

This could cause more reactions (higher volume) and prevent loss processes at the surface (smaller surface). As mentioned before, the gas flow besides the plasma could further reduce losses on the walls and therefore improve the reaction conditions further. The last aspect can be investigated by utilising wider electrodes so that the plasma fills the whole (wide) capillary.

Additionally, the hydrogen peroxide concentration in the liquid increases linearly with the total gas flow, which can be attributed to a higher particle flux. That relation can be obtained by solving equation (4.3) for the hydrogen peroxide concentration

$$c_{\mathrm{H_2O_2}}[\mathrm{mM}] = \frac{n_{\mathrm{H_2O_2}}\phi_{\mathrm{total}}t_{\mathrm{treat}}}{V_{\mathrm{liq}}N_{\mathrm{A}}} \tag{4.4}$$

which depends linearly on the hydrogen peroxide density in the gas phase $n_{\mathrm{H_2O_2}}$ and the total gas flow ϕ_{total}. Moreover, equation (4.4) describes a linear dependence of the hydrogen peroxide concentration on the treatment time t_{treat} which was discussed at the beginning of this chapter (see figure 4.1). It was expected that the hydrogen peroxide concentration increases with the total gas flow as reported by Vasko et al. [38]. However, the increase was not caused by the decreasing residence time but rather the increasing particle flux. This was not considered by Vasko et al. and gives an insight into the dependencies of the hydrogen peroxide concentration in the liquid. Nevertheless, a small influence of the residence time on the hydrogen peroxide density in the gas was observed which should be investigated further. Another aspect that was not considered is the cooling of the electrodes by the total gas flow which should increase with the latter. Vasko et al. measured the gas temperature and found a maximum variation of 30 K [38]. Additionally, the thermal dissociation of hydrogen peroxide possesses rates several magnitudes lower than other loss processes [38]. Therefore, the observed increase in hydrogen peroxide concentration should not be caused by cooling of the electrodes.

4.5 Frequency modulation (RQ5)

The goal of the frequency modulation was to accumulate the long-lived hydrogen peroxide in the plasma, while the density of short-lived species, such as hydroxyl, decreases [7]. In doing so, the destruction of hydrogen peroxide by hydroxyl is prevented as the main loss process requires hydroxyl (see section 2.2). To effect production and loss processes in the plasma, the frequency modulation needs to occur while a set of particles transverses the plasma volume. Therefore, the periods of the modulation ($T = 1/f$ with the frequency f) were chosen around the residence time of the species in the plasma (2.4 ms, for $\phi_{\mathrm{total}} = 1\,\mathrm{slm}$). The RF frequency was modulated by operating the generator with a rectangle pulse. Hereby, several frequencies and two duty cycles were investigated. Before the measurements the power was set to 6 W without frequency modulation. During the measurement the power was not readjusted as it can only be determined in post processing. The frequency modulation lies in the magnitude of milliseconds and one RF cycle (13.56 MHz) lasts about 74 ns. As the oscilloscope trigger was set to the modulating signal and the output for a whole pulse was saved, the resolution of the data was too low to determine the phase shift between voltage and current accurately. Therefore it was not possible to determine the power, which was applied during the frequency modulation measurements, in post processing. However, it is assumed that the power amounted to about 6 W as it was not readjusted. This refers to the power when the plasma is ignited and not the average power according to the duty cycle. The concentration of water vapour in the gas flow amounted to (6700 ± 300) ppm in every measurement and the treatment time was 5 min.

In the following, the dependency of the hydrogen peroxide concentration on the frequency modulation is discussed. To compare different frequencies and duty cycles, the number of pulses per residence time is introduced:

$$N_{\text{pulse}} = \frac{T_{\text{residence}}}{T_{\text{pulse}}} = T_{\text{residence}} \times f_{\text{pulse}} \tag{4.5}$$

with the pulse period T_{pulse}, the residence time $T_{\text{residence}}$ and the pulse frequency f_{pulse}. In figure 4.10 the hydrogen peroxide concentration is shown as function of the number of pulses per residence time. The grey bar depicts the hydrogen peroxide concentration for the same parameters but without frequency modulation. It can be seen that the hydrogen peroxide concentration increases up to about 0.4 mM with the number of pulses per residence time for a duty cycle of 10 %. For a duty cycle of 50 % the hydrogen peroxide concentration is constant around 0.7 mM. Hence, the expected effect of pulse-wise hydrogen peroxide accumulation in the plasma volume cannot be seen for the investigated pulse periods with a duty cycle of 50 %. However, with the duty cycle set to 10 % the hydrogen peroxide concentration increases with the number of pulses per residence time. Further measurements for 4 or 5 pulses per residence time could clarify the trend of the hydrogen peroxide concentration seen in figure 4.10. Possibly the hydrogen peroxide concentration decreases for even higher pulses per residence when their periods approach the time the generator needs to ramp-up the power.

Even if the overall hydrogen peroxide concentration is lower in pulsed than in normal mode, the frequency modulation offers higher energy efficiency due to shorter on-times of the plasma. For example, with a duty cycle of 50 % the plasma is turned on only half of the time. Nevertheless, the hydrogen peroxide concentration is almost as high as the concentration reached without modulation of the frequency. Figure 4.11 shows the energy yield as function of the number of pulses. With frequency modulation the energy yield is indeed higher. A maximal energy yield of about 0.73 mg kWh^{-1} is reached for the duty cycle set to 10 % and 3 pulses per residence time. This is about three orders of magnitude lower than the energy yield of 0.12 g kWh^{-1} reported by Vasko et al. In sum, the modulation of the frequency can be applied to minimize the dissipated energy, but it needs further investigation to fully understand it. Especially, a duty cycle of 10 % at higher number of pulses per residence time could increase the energy yield. Another possibility is to decrease the duty cycle even further.

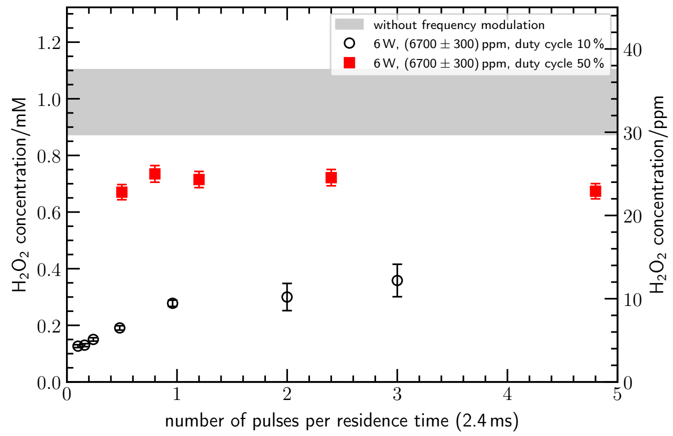

Figure 4.10: Hydrogen peroxide concentration depending on the number of pulses per residence time at a power of 6 W during on-time (determined prior to measurements) and a water admixture of (6700 ± 300) ppm. The average hydrogen peroxide concentrations obtained with the spectrophotometric method after 5 min treatment time and with a total gas flow of 1 slm are used. The measurements for 2 and 3 pulses per residence time were conducted after readjusting the jet. Thus, the corresponding uncertainty was applied.

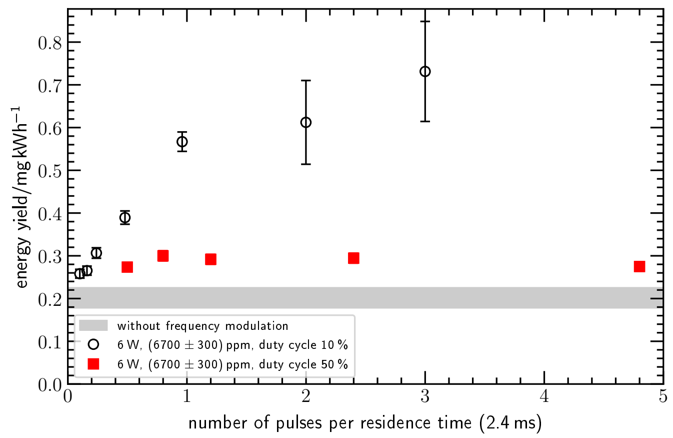

Figure 4.11: Energy yield of hydrogen peroxide depending on the number of pulses per residence time at a power of 6 W (determined prior to measurements) and a water admixture of (6700 ± 300) ppm. The average hydrogen peroxide concentrations obtained with the spectrophotometric method after 5 min treatment time and with a total gas flow of 1 slm are used. The measurements for 2 and 3 pulses per residence time were conducted after readjusting the jet. Thus, the corresponding uncertainty was applied.

4.6 Evaporation

To evaluate if evaporation affects the results discussed above, it was measured by determining the weight difference prior to and after the plasma treatment. Evaporation could influence the hydrogen peroxide concentration by decreasing the liquid volume and thus increasing the hydrogen peroxide concentration in the liquid. Hereby, it is assumed that only the water in the liquid evaporates but other species such as hydrogen peroxide do not. Additionally, these measurements provide information for the application in biocatalysis.

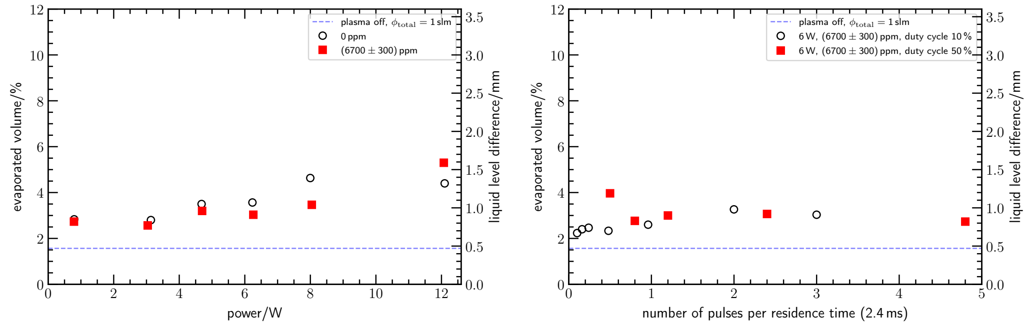

Figure 4.12: The standardized evaporated volume (left y-axis) and the liquid level difference (right y-axis) as function of the power (left) and number of pulses per residence time (right). Exemplary, the measurements for water concentration of 0 ppm and (6700 ± 300) ppm are compared (left). The total gas flow amounted to 1 slm. Measurement uncertainties are omitted due to their small magnitude (0.03 % evaporated volume).

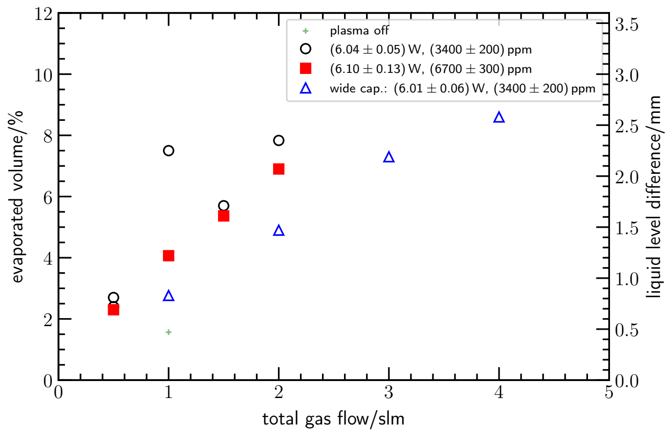

Figure 4.13: The standardized evaporated volume (left y-axis) and the liquid level difference (right y-axis) as function of the total gas flow. Measurement uncertainties are omitted due to their small magnitude (0.03 % evaporated volume).

The relation between the evaporated volume of the liquid and the power, frequency modulation and the total gas flow was analysed and is presented in figure 4.12 and

4.13. As reference, the evaporated volume was measured for a total gas flow of 1 slm while the plasma was turned off. The evaporated volume increases with power but there are only small differences regarding the variation of water admixtures (see figure 4.12, left). The maximal evaporated volume for a power of 12 W, a water concentration of (6700 ± 300) ppm and a total gas flow of 1 slm amounts to about 5.5 %. If the frequency is modulated, the evaporated volume is lower than 4 % of the volume for all measurements. The evaporated volume with frequency modulation coincides with the evaporation of about 3 % for measurements without frequency modulation at 6 W and (6700 ± 300) ppm. As for the power, the evaporated volume increases with the total gas flow up to about 8.5 % at a total gas flow of 4 slm through the wide capillary (see figure 4.13). As stated above, the evaporated volume for plasma treatments with and without frequency modulation is similar, although the average power is lower in measurements with frequency modulation. This can be explained by the stronger influence of the total gas flow on the evaporated volume compared to the power. This is supported by the evaporated volume when the plasma is turned off, which amounts to about half of the evaporated volume in most of the power measurements (see figure 4.12). Moreover, the difference between the evaporated volume with and without plasma for a total gas flow of 1 slm suggests a not identified measurement uncertainty. As the uncertainties induced by the scale are negligible (0.03 %), this should be considered in further investigations.

In sum, increasing the total gas flow yields higher hydrogen peroxide concentrations but more evaporation. However, due to the generally low evaporated volume (< 8.5 %) evaporation does not impact the results discussed above. Considering the dependency of the hydrogen peroxide concentration on the total gas flow, if evaporation had a noticeable effect, the slope of this curve should increase with the total gas flow. This can not be seen in figure 4.7 as the curve is linear. Therefore, the neglect of the evaporation is justified. However, for long treatment times and the application in biocatalysis evaporation should be considered.

5 Conclusion and Outlook

In this work, different parameters of the plasma source were varied and the effects on the hydrogen peroxide concentration are reported. In order to produce the most hydrogen peroxide with the capillary jet the following should be considered:

- Use helium instead of argon as working gas.
- Set the dissipated power in the plasma to around 6 W.
- Use the highest possible water concentration (6700 ± 300) ppm corresponding to 100 % gas flow through the bubbler system.
- Use the highest possible total gas flow (small: 2 slm, wide capillary: 4 slm).
- Use the wide capillary instead of the small capillary.
- Modulate the frequency to achieve a high number of pulses per residence time to improve the energy efficiency.

The presented results answer the research questions stated in section 2.3. The variation of power (RQ1) and water admixture (RQ2) revealed that the hydrogen peroxide concentration stagnates for powers higher than 6 W. Concerning the water admixture, the expected linear dependency of the hydrogen peroxide concentration was not observed. Towards higher water concentrations the slope of that curve decreased further. This is not consistent with the results of Vasko et al. [38] but the curve matches results of Schröter [31]. In general, the deviation from the linear dependency could be attributed to hydroxyl as well as to changes in electron density and temperature (see section 4.2). With respect to RQ3, which refers to the working gas, the use of helium yields higher hydrogen peroxide concentrations and a more stable discharge (see section 4.3). To explain this result, additional information, such as the gas and electron temperature as well as the electron density, is needed due to the dependency of the rate coefficients on these parameters (see section 2.2).

Related to RQ4, the hydrogen peroxide concentration increases linearly with the total gas flow and the treatment time (see section 4.4). This can be attributed to the increasing particle flux and not, as expected, to the residence time. Moreover, the hydrogen peroxide concentration depends weakly on the residence time which contradicts findings of Vasko et al. [38]. Additionally, the small and wide capillary were compared and with the latter more hydrogen peroxide is produced under comparable conditions. Finally, the frequency modulation (RQ5) proved to be interesting for possible scale ups of the biocatalysis setup due to its higher energy yield (see section 4.5). Furthermore, the measurement of the evaporation showed that it increases with the power and the total gas flow. However, the dependence on the latter is stronger. Distinct water admixtures exhibited little to no impact on the evaporated volume. Generally, the evaporation did not affect the hydrogen peroxide concentration due to the low evaporated volumes. Regarding the electrochemical probe, an improved version will be applied in future measurements to validate the absolute values of the spectrophotometric method.

In sum, the determination of the electron density and temperature as well as the gas temperature could validate the hypothesized reasons for changes in the hydrogen peroxide concentration. Also the concentrations of other reactive species such as hydroxyl are to be determined because the enzymes can suffer from inactivation if in contact with those species. On the other hand, the whole pathway of hydrogen peroxide from the plasma, over the effluent to the liquid needs to be considered to validate if the hydrogen peroxide concentration in the plasma corresponds to the observed concentration in the liquid. As the latter was determined successfully in this work, the concentrations of reactive species in the plasma and the effluent are yet to be investigated.

Bibliography

[1] O. A. Alduchov and R. E. Eskridge, *Improved magnus‘ form approximation of saturation vapor pressure*, DOE/ER/61011-T6 (Department of Commerce, Asheville, NC (United States), 1st Nov. 1997).

[2] J. Benedikt, D. Schröder, S. Schneider, G. Willems, A. Pajdarová, J. Vlček and V. Schulz-von der Gathen, ‘Absolute OH and o radical densities in effluent of a he/H_2O micro-scaled atmospheric pressure plasma jet’, Plasma Sources Science and Technology **25**, 045013 (2016).

[3] L. Bischoff, G. Hübner, I. Korolov, Z. Donkó, P. Hartmann, T. Gans, J. Held, V. Schulz-von der Gathen, Y. Liu, T. Mussenbrock and J. Schulze, ‘Experimental and computational investigations of electron dynamics in micro atmospheric pressure radio-frequency plasma jets operated in He/N_2 mixtures’, Plasma Sources Science and Technology **27**, 125009 (2018).

[4] P. J. Bruggeman, M. J. Kushner, B. R. Locke, J. G. E. Gardeniers, W. G. Graham, D. B. Graves, R. C. H. M. Hofman-Caris, D. Maric, J. P. Reid, E. Ceriani, D. Fernandez Rivas, J. E. Foster, S. C. Garrick, Y. Gorbanev, S. Hamaguchi, F. Iza, H. Jablonowski, E. Klimova, J. Kolb, F. Krcma, P. Lukes, Z. Machala, I. Marinov, D. Mariotti, S. Mededovic Thagard, D. Minakata, E. C. Neyts, J. Pawlat, Z. L. Petrovic, R. Pflieger, S. Reuter, D. C. Schram, S. Schröter, M. Shiraiwa, B. Tarabová, P. A. Tsai, J. R. R. Verlet, T. von Woedtke, K. R. Wilson, K. Yasui and G. Zvereva, ‘Plasma–liquid interactions: a review and roadmap’, Plasma Sources Science and Technology **25**, 053002 (2016).

[5] P. Bruggeman and D. C. Schram, ‘On OH production in water containing atmospheric pressure plasmas’, Plasma Sources Science and Technology **19**, 045025 (2010).

[6] F. F. Chen, *Introduction to plasma physics and controlled fusion* (Springer International Publishing, Cham, 2016).

[7] Collaborative Research Center 1316, *CRC1316 proposal for the second funding period* (Ruhr-Universität Bochum, 2021).

[8] R. Forster, M. Frost, D. Fulle, H. F. Hamann, H. Hippler, A. Schlepegrell and J. Troe, ‘High pressure range of the addition of HO to HO, NO, NO2, and CO. i. saturated laser induced fluorescence measurements at 298 k’, The Journal of Chemical Physics **103**, Publisher: American Institute of Physics, 2949–2958 (1995).

[9] M. Girhard, E. Kunigk, S. Tihovsky, V. V. Shumyantseva and V. B. Urlacher, 'Light-driven biocatalysis with cytochrome p450 peroxygenases', Biotechnology and Applied Biochemistry **60**, 111–118 (2013).

[10] J. Golda, J. Held and V. S.-v. d. Gathen, 'Comparison of electron heating and energy loss mechanisms in an RF plasma jet operated in argon and helium', Plasma Sources Science and Technology **29**, 025014 (2020).

[11] J. Golda, J. Held, B. Redeker, M. Konkowski, P. Beijer, A. Sobota, G. Kroesen, N. S. J. Braithwaite, S. Reuter, M. M. Turner, T. Gans, D. O'Connell and V. Schulz-von der Gathen, 'Concepts and characteristics of the 'COST reference microplasma jet'', Journal of Physics D: Applied Physics **49**, 084003 (2016).

[12] J. Golda, F. Kogelheide, P. Awakowicz and V. S.-v. d. Gathen, 'Dissipated electrical power and electron density in an RF atmospheric pressure helium plasma jet', Plasma Sources Science and Technology **28**, 095023 (2019).

[13] Y. Gorbanev, C. C. W. Verlackt, S. Tinck, E. Tuenter, K. Foubert, P. Cos and A. Bogaerts, 'Combining experimental and modelling approaches to study the sources of reactive species induced in water by the COST RF plasma jet', Physical Chemistry Chemical Physics **20**, 2797–2808 (2018).

[14] Y. Gorbanev, D. O'Connell and V. Chechik, 'Non-thermal plasma in contact with water: the origin of species', Chemistry - A European Journal **22**, 3496–3505 (2016).

[15] Y. Gorbanev, A. Privat-Maldonado and A. Bogaerts, 'Analysis of short-lived reactive species in plasma–air–water systems: the dos and the do nots', Analytical Chemistry **90**, 13151–13158 (2018).

[16] T. Hemke, D. Eremin, T. Mussenbrock, A. Derzsi, Z. Donkó, K. Dittmann, J. Meichsner and J. Schulze, 'Ionization by bulk heating of electrons in capacitive radio frequency atmospheric pressure microplasmas', Plasma Sources Science and Technology **22**, 015012 (2012).

[17] Y. Itikawa and N. Mason, 'Cross sections for electron collisions with water molecules', Journal of Physical and Chemical Reference Data **34**, Publisher: American Institute of Physics, 1–22 (2005).

[18] J. Jankunas, B. Bertsche, K. Jachymski, M. Hapka and A. Osterwalder, 'Dynamics of gas phase $Ne^* + NH_3$ and $Ne^* + ND_3$ penning ionisation at low temperatures', The Journal of Chemical Physics **140**, 244302 (2014).

[19] J. Jonkers, M. v. d. Sande, A. Sola, A. Gamero and J. v. d. Mullen, 'On the differences between ionizing helium and argon plasmas at atmospheric pressure', Plasma Sources Science and Technology **12**, 30–38 (2003).

[20] D. Jung, C. Streb and M. Hartmann, 'Oxidation of indole using chloroperoxidase and glucose oxidase immobilized on SBA-15 as tandem biocatalyst', Microporous and Mesoporous Materials **113**, 523–529 (2008).

[21] A. A. Karyakin, 'Prussian blue and its analogues: electrochemistry and analytical applications', Electroanalysis **13**, 813–819 (2001).

[22] A. A. Karyakin and E. E. Karyakina, 'Prussian blue-based 'artificial peroxidase' as a transducer for hydrogen peroxide detection. application to biosensors', Sensors and Actuators B: Chemical **57**, 268–273 (1999).

[23] K. Lee and S.-H. Moon, 'Electroenzymatic oxidation of veratryl alcohol by lignin peroxidase', Journal of Biotechnology **102**, 261–268 (2003).

[24] M. A. Lieberman and A. J. Lichtenberg, *Principles of plasma discharges and materials processing*, 2nd ed, OCLC: ocm56752658 (Wiley-Interscience, Hoboken, N.J, 2005), 757 pp.

[25] D. X. Liu, P. Bruggeman, F. Iza, M. Z. Rong and M. G. Kong, 'Global model of low-temperature atmospheric-pressure He + H_2O plasmas', Plasma Sources Science and Technology **19**, 025018 (2010).

[26] J. A. Manion, R. E. Huie, R. D. Levin, D. R. J. Burgess, V. L. Orkin, W. Tsang, W. S. McGivern, J. W. Hudgens, V. D. Knyazev, D. B. Atkinson, E. Chai, A. M. Tereza, C.-Y. Lin, T. C. Allison, W. G. Mallard, F. Westley, J. T. Herron, R. F. Hampson and D. H. Frizzell, *NIST chemical kinetics database*, NIST Standard Reference Database 17, Version 7.0 (Web Version), Release 1.6.8, Data version 2015.09, (17th May 2022) `https://kinetics.nist.gov/`.

[27] M. Moravej, X. Yang, G. R. Nowling, J. P. Chang, R. F. Hicks and S. E. Babayan, 'Physics of high-pressure helium and argon radio-frequency plasmas', Journal of Applied Physics **96**, 7011–7017 (2004).

[28] R. Nogueira, M. Oliveira and W. Paterlini, 'Simple and fast spectrophotometric determination of H2O2 in photo-fenton reactions using metavanadate', Talanta **66**, 86–91 (2005).

[29] J. R. Roth, *Industrial plasma engineering* (Institute of Physics Pub, Bristol ; Philadelphia, 1995), 1 p.

[30] A. Schmid, J. S. Dordick, B. Hauer, A. Kiener, M. Wubbolts and B. Witholt, 'Industrial biocatalysis today and tomorrow', Nature **409**, 258–268 (2001).

[31] S. Schröter, 'Reactive oxygen and hydrogen species generation in radio-frequency atmospheric pressure plasmas', 177.

[32] V. Schulz-von der Gathen, L. Schaper, N. Knake, S. Reuter, K. Niemi, T. Gans and J. Winter, 'Spatially resolved diagnostics on a microscale atmospheric pressure plasma jet', Journal of Physics D: Applied Physics **41**, 194004 (2008).

[33] R. A. Sheldon, 'Biocatalysis and green chemistry', in *Green biocatalysis*, Section: 1 _eprint: https://onlinelibrary.wiley.com/doi/pdf/10.1002/9781118828083.ch1 (John Wiley & Sons, Ltd, 2016), pp. 1–15.

[34] Y. Shiraishi, S. Kanazawa, D. Tsukamoto, A. Shiro, Y. Sugano and T. Hirai, 'Selective hydrogen peroxide formation by titanium dioxide photocatalysis with benzylic alcohols and molecular oxygen in water', ACS Catalysis **3**, Publisher: American Chemical Society, 2222–2227 (2013).

[35] D. F. Swinehart, 'The beer-lambert law', Journal of Chemical Education **7**, 3 (1962).

[36] C. Tendero, C. Tixier, P. Tristant, J. Desmaison and P. Leprince, 'Atmospheric pressure plasmas: a review', Spectrochimica Acta Part B: Atomic Spectroscopy **61**, 2–30 (2006).

[37] F. Tochikubo, S. Uchida and T. Watanabe, 'Study on decay characteristics of OH radical density in pulsed discharge in Ar/H_2O', Japanese Journal of Applied Physics **43**, 315–320 (2004).

[38] C. A. Vasko, D. X. Liu, E. M. van Veldhuizen, F. Iza and P. J. Bruggeman, 'Hydrogen peroxide production in an atmospheric pressure RF glow discharge: comparison of models and experiments', Plasma Chemistry and Plasma Processing **34**, 1081–1099 (2014).

[39] J. L. Walsh, F. Iza, N. B. Janson, V. J. Law and M. G. Kong, 'Three distinct modes in a cold atmospheric pressure plasma jet', Journal of Physics D: Applied Physics **43**, Publisher: IOP Publishing, 075201 (2010).

[40] J. Winter, R. Brandenburg and K.-D. Weltmann, 'Atmospheric pressure plasma jets: an overview of devices and new directions', Plasma Sources Science and Technology **24**, 064001 (2015).

[41] T. Winzer, N. Blosczyk, J. Benedikt and J. Golda, 'Multi-diagnostic approach to energy transport in an atmospheric pressure helium-oxygen plasma jet', arXiv:2102.12126 [physics], `10.48550/arXiv.2102.12126` (2021).

[42] J. Yang, M. Lin, M. Cho and Y. Lee, 'Determination of hydrogen peroxide using a prussian blue modified macroporous gold electrode', Microchimica Acta **182**, 1089–1094 (2015).

[43] X. Yang, M. Moravej, G. R. Nowling, S. E. Babayan, J. Panelon, J. P. Chang and R. F. Hicks, 'Comparison of an atmospheric pressure, radio-frequency discharge operating in the α and γ modes', Plasma Sources Science and Technology **14**, 314–320 (2005).

[44] A. Yayci, Á. G. Baraibar, M. Krewing, E. F. Fueyo, F. Hollmann, M. Alcalde, R. Kourist and J. E. Bandow, 'Plasma-driven in situ production of hydrogen peroxide for biocatalysis', ChemSusChem **13**, 2072–2079 (2020).

[45] A. Yayci, T. Dirks, F. Kogelheide, M. Alcalde, F. Hollmann, P. Awakowicz and J. E. Bandow, 'Microscale atmospheric pressure plasma jet as a source for plasma-driven biocatalysis', ChemCatChem **12**, 5893–5897 (2020).